의학박사 학위논문

Effect of IL-4, type I interferon, and IL-15 on the development and function of virtual memory CD8 T cells

인터루킨-4, 제1형 인터페론 그리고 인터루킨-15가 가상기억 CD8 T 세포의 발달과 기능에 미치는 영향

2023년 08월

서울대학교 대학원

의학과 중개의학전공

박 희 정

인터루킨-4, 제1형 인터페론 그리고 인터루킨-15가 가상기억 CD8 T 세포의 발달과 기능에 미치는 영향

Effect of IL-4, type I interferon, and IL-15 on the development and function of virtual memory CD8 T cells

August 2023

The Department of Medicine,
Seoul National University
College of Medicine
Hi Jung Park

Effect of IL-4, type I interferon, and IL-15 on the development and function of virtual memory CD8 T cells

by

Hi Jung Park

(Directed by Prof. Kyeong Cheon Jung)

A Dissertation submitted to the Department of Medicine in partial fulfillment of the requirements for the Degree of Ph.D. of Science in Medicine (Translational Medicine) at Seoul National University College of Medicine

July 2023

Approved by Thesis Committee:

Chair	**Eun Bong Lee**	**(Seal)**
Vice Chair	**Kyeong Cheon Jung**	**(Seal)**
Examiner	**Lee Jae Il**	**(Seal)**
Examiner	**Youn Soo CHOI**	**(Seal)**
Examiner	**Kwonik Oh**	**(Seal)**

인터루킨-4와 제1형 인터페론 그리고 인터루킨-15가 가상기억 CD8 T 세포의 발달과 기능에 미치는 영향

지도 교수 정 경 천

이 논문을 의학박사 학위논문으로 제출함

2023년 4월

서울대학교 대학원

의학과 중개의학

박 희 정

박희정의 의학박사 학위논문을 인준함

2023년 7월

위 원 장 이 은 봉 (인)

부위원장 정 경 천 (인)

위 원 이 재 일 (인)

위 원 최 윤 수 (인)

위 원 오 권 익 (인)

ABSTRACT

Conventional memory T cells typically develop from naïve T cells following exposure to antigenic stimulation and acquisition of memory phenotypes. However, certain CD8 T cells in the thymus, known as “innate T cells” and "virtual memory (VM) CD8 T cells” in the peripheral tissues already exhibit memory-like characteristics such as elevated CD44 expression and rapid cytokine production, even without prior exposure to foreign antigens. This study analyzed the function and development of VM CD8 T cells under the influence of different cytokines.

Consistent with previous studies, administration of exogenous IL-4 complexed with anti-IL-4 antibody (IL-4C) led to the generation and expansion of memory-like CD8 T cells, along with an increase in CXCR3 expression in both naïve- and memory-like cells. Thus, the migration of virus-specific and bystander CD8 T cells, including those with a naïve phenotype, was facilitated into the lung during influenza infection.

To investigate the effect of type I interferon (IFN), IL-4, and IL-15 on the development of VM CD8 T cell subpopulations, VM cells were divided into four subsets based on Ly6C and Sca-1 expression. The development of these subsets was studied using knockout (KO) mice

lacking IFN-α receptor 1 (IFNAR1), IL-4, or IL-15 receptor α (IL-15Rα). The population of Ly6C^{+} Sca-1^{+} and Ly6C^{-} Sca-1^{+} VM CD8 T cells was significantly diminished in the spleen of IFNAR1 KO mice, which were unable to receive type I IFN-stimulated signals, although the total number of splenocytes, CD8 T cells and CD44^{hi} CD49d^{-} VM CD8 T cells were comparable to that of wild-type (WT) mice, due to an increased number of Ly6C^{-} Sca-1^{-} VM cells. Conversely, the proportion of Ly6C^{+} Sca-1^{-} VM CD8 T cells was partially reduced in IL-4 KO mice, resulting in an overall decrease in the total VM CD8 T cell fraction. Both the Ly6C^{+} Sca-1^{-} and Ly6C^{+} Sca-1^{+} VM CD8 T cell subsets were significantly reduced in the spleen of IL-15Rα KO mice. These findings highlight the differential effects of type I IFN, IL-4, and IL-15 cytokines on the development of distinct subsets of VM CD8 T cells.

Bulk RNA sequencing analysis of different CD8 T cell subsets, including naïve cells, true memory cells, and four subsets of VM cells, uncovered distinct gene expression patterns. Ly6C^{+} VM CD8 T cells were enriched with IL-15 signal-related genes such as *Il2rb* and *Il15ra*, as well as memory-related genes like *Runx2* and *Eomes*. However, Ly6C^{-} VM cells, along with true memory CD8 T cells, were enriched cell cycle-related genes. In particular, the expression of the *Mst1* gene, known to promote cellular quiescence and survival in type I invariant NKT cells (iNKT1) cells upon IL-15 stimulation, was higher in Ly6C^{+} VM cells

compared with other CD8 T cell subsets. This finding correlated with the increased dependency of Ly6C^{+} VM cells on IL-15 for their survival.

Overall, this study demonstrated the heterogeneity of VM CD8 T cells, and their development was affected differentially by type I IFN, IL-4, and IL-15 cytokines. In addition, the upregulation of CXCR3 on VM CD8 cells facilitated their migration to inflammatory sites.

Keywords: IL-4, Type I IFN, IL-15, VM CD8 T cells, IAV, CXCR3

Student number: 2016-30010

CONTENTS

LIST OF FIGURES

LIST OF TABLES

LIST OF ABBREVIATIONS

7-AAD : 7-Aminoactinomycine D

AM : Alveolar Macrophage

B6 : C57BL/6

CD : Cluster differentiation

CXCR3 : chemokine (C-X-C motif) receptor 3

Eomes : Eomesodermin

Eosino : Eosinophil

GSEA : Gene Set Enrichment Analysis

IFNAR1: Type I Interferon receptor alpha 1

IL-15Rα : Interleukin-15 receptor alpha

IL-4C : Interleukin-4 and anti-interleukin-4 antibody complex

IL : Interleukin

iMono : inflammatory monocyte

KO : knock-out

LN : Lymph node

Ly6C : Lymphocyte antigen 6 family member C

Neutro : Neutrophil

Sca-1 : Stem cells antigen-1

SPL : Spleen

TM: true memory

VM : Virtual memory

WT : WILD-TYPE

INTRODUCTION

During the development of conventional T cells in the thymus, $CD4^+CD8^+$ (double positive) thymocytes express the memory T cell marker CD44 (in mice) or CD45RO (in humans) after positive selection, followed by conversion to $CD44^{low}$ (in mice) or $CD45RA^+$ (in humans) naïve phenotype during the terminally differentiated single positive ($CD4^+CD8^-$ or $CD4^-CD8^+$) stage. In the peripheral lymphoid organs, these T cells are exposed to agonistic antigens and turn into effectors, followed by differentiation into memory T cells. However, some of the T cells in the thymus, known as "innate T cells" still express memory phenotype [1]. The prototype of these types of antigen inexperienced memory-like T cells are non-classical MHC class Ib-restricted innate T cells, such as natural killer T (NKT), mucosal-associated invariant T (MAIT) and H2-M3-specific CD8 T cells, which recognize antigens presented by CD1d, MR-1 and H2-M3 molecules, respectively, during early immune responses [1-3]. These cells carry substantially less diverse T cell receptor (TCR) repertoire than conventional T cells. However, some of the antigen inexperienced memory-like T cells are derived from CD8 T cells that are positively selected by the MHC class I/self-peptide complex. They exhibit a more diverse TCR repertoire and generate cytokines upon TCR stimulation, similar to a conventional memory T cells [4-7].

Such innate CD8 T cells have been identified in a mouse model lacking Itk, Rlk, Klf2, Cbp or Id3 and acquire memory phenotypes such as CD44, CD122 (IL-2/IL-15Rβ, common receptor for IL-2 and IL-15), Eomesodermin (Eomes) and CXCR3 in the thymus [3, 8-10]. These cells were also found in wild-type (WT) mice such as the BALB/c strain. The development of these $Eomes^+$ innate CD8 cells depends on interleukin-4 (IL-4), which is produced by NKT cells in the thymus of WT and most of the genetically modified mice [8]. In addition, type I interferon (IFN) has also been reported to induce the development of $Eomes^+$ innate CD8 cells [7].

$Eomes^+$ innate CD8 cells are rarely encountered in the thymus of WT mice [7, 8]. However, mice have a significant number of CD8 T cells with memory phenotype in their lymphoid organs, even under germ-free conditions, suggesting that these cells can acquire a memory phenotype in the absence of antigen exposure [11-14]. These CD8 T cells are commonly referred to as "virtual memory" (VM) CD8 T cells [4]. In humans, $CD45RA^+KIR/NKG2a^+$ $Eomes^+$ CD8 T cells, which have been detected in both umbilical cord blood and adult peripheral blood, are similar to mouse VM T cells [15, 16].

VM CD8 T cells in mice have been phenotypically defined as $CD44^{hi}$ $CD49d^-$ CD8 T cells, using CD49d as a marker to exclude true

memory (TM) cells [4, 12]. VM CD8 T cells arise from innate CD8 T cells generated in the thymus [17]. CXCR3 is a chemokine receptor with a significant impact on T cell trafficking and function [18]. CXCR3 is highly expressed in IL-4-induced CD8 innate T cells, along with CD44, CD122 and Eomes [8]. Further, the peripheral CD8 T cells decreased in IL-4Rα KO mice exhibit a $CD44^{hi}$ $CXCR3^{+}$ phenotype [19]. Conversely, the administration of exogenous IL-4 to mice resulted in the development and expansion of $CD44^{hi}$ $CXCR3^{+}$ CD8 T cell populations in both thymus and peripheral lymphoid organs [17, 20, 21]. However, it has been shown that type I IFN-dependent memory-like CD8 T cells also express high levels of CXCR3 [7]. This suggests that CXCR3 expression may not be a reliable marker for distinguishing IL-4-dependent from type I IFN-dependent memory-like CD8 T cells.

In addition, VM CD8 T cells are also generated in T-cell lymphopenia, a condition characterized by abnormally low levels of lymphocytes or in response to cytokines such as IL-4, type I IFN and IL-15 [4-6, 22]. Specifically, IL-4Rα knock-out (KO) mice showed a reduction in the population of peripheral memory-like CD8 T cells [19]. $CD44^{hi}$ $CD49d^{-}$ VM CD8 T cells were found to be reduced in the spleen of IRF9 KO mice, which lack type I IFN signaling [7]. However, IL-15 is not only essential for the development of IL-4-induced innate CD8 T cells [1], but also for the expansion of VM CD8 T cells. The development

of VM cells from naive CD8 T cells via homeostatic proliferation depend on the presence of IL-15, and the administration of exogenous IL-15, as well as IL-15 overexpression in transgenic mice, leads to an increase in VM CD8 T cell population [9, 13]. Therefore, IL-4, type I IFN, and IL-15 are the only cytokines reported to date during the development and expansion of VM CD8 T cells. However, the specific interaction between these three cytokines in VM CD8 T cells have yet to be fully elucidated.

Sca-1 (stem cell antigen-1) and Ly6C (lymphocyte antigen 6 complex, locus C) are surface markers that can be used to identify the T cell differentiation stage [23]. In CD8 T cells, Sca-1 is typically not expressed in naïve T cells, while Ly6C is expressed at low levels and its expression in naïve cells has been reported to be influenced by type I IFN signaling [23, 24]. The two major subsets of $CD8^+$ memory T cells in mice include: $CD44^{hi}CD62L^{lo}$, also known as effector memory T cells, and $CD44^{hi}CD62L^{hi}$, also known as central memory T cells. The effector memory T-cell subset expresses high levels of Sca-1, whereas the central memory T-cell subset carries elevated levels of Ly6C [23]. Further, Sca-1 expression in T cells is upregulated by type I IFN signaling [23, 25]. Although Sca-1 and Ly6C have been implicated in T cell activation and proliferation, the precise effects of cytokines on VM CD8 T cells in relation to their Sca-1 and Ly6C expression patterns are incompletely understood.

Influenza A is an RNA virus known for its high mutation rate. Each year, new strains of mutated influenza viruses emerge and spread rapidly around the world. This results in significant mortality and morbidity. Despite extensive efforts, the development of well-matched vaccines remains a challenge due to the constant mutation of the virus [26, 27]. Moreover, our fight against viral infections has become more complicated with the emergence of novel, such as MERS (Middle East Respiratory Syndrome) and COVID-19 (Coronavirus disease 2019). These circumstances have prompted the exploration of alternative strategies to provide immediate protection against any pathogen, regardless of its specific type. Such an approach could effectively protect humans from emerging viral infections. One potential strategy involves the use of IL-4- induced innate CD8 T cells, which have been shown to protect mice infected with leukocyte choriomeningitis virus (LCMV) clone 13 from progression to the chronic stage [28]. In this context, activation and expansion of virtual memory CD8 T cell population may be a candidate for this protective strategy.

The aim of this study was to investigate how cytokines, including IL-4, type I IFN and IL-15, affect the development and function of VM CD8 T cells. Toward this end, the protective effects of exogenous IL-4 administration against lethal influenza infection in mice were first investigated, focusing on VM CD8 T cells. Subsequently, the VM CD8

T cells were divided into four subsets based on the expression of Ly6C and Sca-1, and the dependency of the VM cell subsets on each cytokine was identified using KO mouse models. Bulk RNA sequencing analysis and in vitro studies were used to further characterize each VM CD8 T cell. The findings suggest that IL-15-dependent $Ly6C^{+}$ VM CD8 T cells exhibit phenotypic and functional characteristics of memory-like cells.

MATERIALS AND METHODS

1. Mice

C57BL/6 were purchased from Koatech (Pyeongtaek, Korea) and the Jackson Laboratory (Bar Harbor, E, USA). Type I IFN receptor a-chain (IFNAR1) KO were provided by Dr. Nam-Hyuk Cho (Seoul National University College of Medicine). IL-4 $^{-/-}$ and IL-15Ra$^{-/-}$ mice were kindly gifted from Dr. DooHyun Chung (Seoul National University College of Medicine). All mice were bred and maintained under specific pathogen-free conditions in the animal care facilities of the Biomedical Center for Animal Resource Development of Seoul National University, the Institute for Experimental Animals at college of medicine of Seoul National University and the Seoul National University Hospital Biomedical Research Institute. The mice were housed in groups of up to 5 mice per cage with a temperature set point of 22 ±1℃ and a humidity level of 50±10%. All Experiments were approved by the Institutional Animal Care and Use Committee (IACUC) and Institutional Biosafety Committee (IBC) at Seoul National University and Seoul National University Hospital (SNUH), Korea.

2. Antibodies and flow cytometric analysis

Single-cell suspensions of lungs, lymph nodes, and spleens were prepared. The lungs were placed in 5 mL of RPMI-1640 medium containing 1 mg/mL type IV collagenase (Worthington Biochemical Corp, Lakewood, NJ, USA) and 0.05 mg/mL DNAse I (Sigma-Aldrich, St. Louis, MO, USA) and incubated at 37°C for 1 h. The pelleted cells were resuspended in 1 mL of Red Blood Cell Lysing buffer (Sigma-Aldrich) and washed. Fluorochrome-tagged monoclonal antibodies were purchased from BD Bioscience (San Jose, CA, USA), BioLegend (San Diego, CA, USA) or eBioscience (San Diego, CA, USA): Anti-CD3 (145–2C11, 17A2), anti-CD4 (RM4–5), anti-CD8 (53–6.7), anti-TCR (H57-597), anti-CD19 (1D3/CD19), anti-LY49C/H/I/F (14B11), anti-CD49d (R1-2), anti-Sca-1 (D7), anti-CD44 (IM7), anti-CD5 (Ly-1), anti-CD122 (TM-b1), anti-CXCR3 (CXCR3–173), anti-EOMES (Dan11mag), anti-CD11b (M1/70), anti-Ly6C (HK1.4), anti-CCR2 (475301), anti-Gr-1 (RB6.8C5), anti-Siglec F (E50–2440), and anti-CD11c (HL3), anti-IFNr (XMG1.2), anti-TNF alpha (MP6-XT22), anti-granzyme B (NGZB), anti-perforin (S16009A), anti-rabbit IgG (Poly4064), Phospho-MOB1 (Thr35)(D2F10). Influenza virus-specific CD8 T cells were detected using biotin-labeled H-2Db/NP366–374 (ASNENMETM) and PA224–233 (SSLENFRAYV) pentamers [29]. Both pentamers were purchased from ProImmune (Oxford, UK). Cells were suspended with antibodies in fluorescence-activated cell sorting

(FACS) buffer (1x PBS with 0.1% [w/v] bovine serum albumin and 0.1% [w/v] sodium azide) for 30 minutes at 4°C

3. Intracellular cytokine assay

Total splenocytes were incubated with Cell Stimulation Cocktail (500x) (eBioscience) in the presence of Golgiplug (BD Bioscience) for 5 hours at 37°C CO_2 incubator. To measure cytokine production by CD8 T cells, 5×10^5 cells were incubated with 1 μg/mL influenza virus NP366–374 peptide (Cosmogenetech, Seoul, Korea), 10 U/mL IL-2 (Peprotech, Princeton, NJ, USA), and 4 μL/6 mL monensin (BD Bioscience) for 5 hours at 37°C in a 5% (v/v) CO_2 incubator. Cultured cells were stained with surface markers and intracellular staining was performed using a mixture of the fixation and permeabilization buffers of the Foxp3 staining kit (eBioscience, San Diego, CA, USA). After staining, samples were analyzed using BD LSRFortessa, LSRII, or LSRFortessa X-20 platforms (Becton-Dickinson, Mountain View, CA, USA) running FlowJo software (Tree Star, Ashland, OR, USA).

4. Administration of IL-4 and anti-IL-4 antibody in vivo

Based on previous reports [20, 21, 30], 1.5 μg mouse IL-4 (Peprotech,

Princeton, NJ, USA) and 7.5 μg antibody (Ab) against mouse IL-4 (11B11; Bio X Cell, West Lebanon, NH, USA) were mixed in 200 μL phosphate buffered saline (PBS) and intraperitoneally injected into mice daily for 7 days. Control mice received only PBS, IL-4, or anti-IL-4 Ab.

5. Influenza Virus Infection

One day after the final injection of IL-4-anti-IL-4 complex, mice were anesthetized with isoflurane and infected intranasally with 6×10^3 plaque-forming units of influenza A/Puerto Rico/8/34 (H1N1, PR8) virus. The influenza A/Puerto Rico/8/34 (PR8) virus was provided by Young Ki Choi (Chungbuk National University of Medicine, KOREA). After 5 days of infection, mice were sacrificed, and the immune cell profiles of the lungs, lymph nodes, and spleens were assessed via flow cytometry.

6. Plaque assay

The virus titration was measured by Plaque assay [31]. Briefly, monolayers of Madin-Darby Canine Kidney (MDCK) cells were prepared in 6-well plate and incubated for 24 hours. Cultured MDCK cells were washed twice at least via PBS and added 100 μl of serial dilution for 1 hour. Infected MDCK cells were washed and added <1%

SeaPlaque™ Agarose (Lonza, Basel, Switzerland) containing 1 μg/ml of L-(tosylamido-2-phenyl) ethyl chloromethyl ketone (TPCK) -trypsin (Thermofisher, Waltham, MA, USA). After 3~4 days of incubation at 37℃, agarose was removed and plates were fixed with 4% formaldehyde solution and stained 0.5% crystal violet (Sigma-Aldrich, St.Louis, MO, USA)

7. Reverse-transcription Quantitative PCR

Lungs were homogenized in 1 mL of TRIzol reagent (ThermoFisher, Waltham, MA, USA). After RNA extraction, cDNA was synthesized using the AccuPower CycleScript RT PreMix (Bioneer, Daejeon, Korea). The PowerUp SYBR™ Green Master Mix (Applied Biosystems, Waltham, MA, USA) was used to perform real-time quantitative PCR. The primers were as follows: IP-10 (CXCL-10) forward 5′-GAC GGT CCG CTG CAA CTG-3′, reverse 5′-CTT CCC TAT GGC CCT CAT TCT-3′ [32] and GAPDH, forward 5′-TCA CCA CCA TGG AGA AGG C-3′, reverse 5′-GCT AAG CAG TTG GTG GTG CA-3′ [33].

8. ELISA

Influenza virus-specific antibodies were measured via ELISA as

described previously [34]. Ninety-six-well plates were coated with 1 µg/mL influenza A H1N1 (A/Puerto Rico/8/1934) hemagglutinin (HA; Sino Biological Inc., Wayne, PA, USA). Plates were blocked with 1× casein solution buffer (Vector Laboratories Inc., Burlingame, CA, USA) for 2 hours at 37°C and washed with PBS-Tween 20 buffer. Then, serum samples were added at two-fold dilutions, followed by incubation for 1 hour and subsequent incubation with anti-mouse IgG HRP (Promega, Madison, WI, USA) for 30 minutes at 37°C. The plates were developed with tetramethylbenzidine (Life technologies, Carlsbad, CA, USA) for 10 min and absorbances at 450 nm were measured using an Epoch device (Biotek, Winooski, VT, USA).

9. RNA extraction

Using anti-CD8 microbeads, CD8 T cells were isolated from the spleens of C57BL/6 by magnetic sorting (MACS; Miltenyi Biotec, Auburn, CA, USA) and sorted into Naïve ($CD44^{-}CD49d^{-}$), TM ($CD44^{+}CD49d^{+}$) and VM ($CD44^{+}CD49d^{-}$) based on the expression of Ly6C and Sca-1, using a BD FACS Aria^{TM}III Cell sorter (BD Bioscience). RNA was extracted using Isolate II RNA mini kit (Meridian Bioscience, OH, USA).

10. Data processing

Library preparation was by the TruSeq Stranded mRNA LT Sample Prep Kit. Paired-end sequencing reads (101bp) generated from Illumina instruments were verified its sequence quality with FastQC (version 0.11.7). Before starting analysis, Trimmomatic (version 0.38) [35] is used to remove adapter sequences and remove bases with base quality lower than 3 from the ends reads. Also using sliding window trim method, bases that does not qualify for window size=4, and mean quality=15 are removed. Afterwards, reads with minimum length of 36bp are removed to produce cleaned data.

11. Aligning reads to reference genome

We preprocessed the raw reads from the sequencer to remove low quality and adapter sequence before analysis and aligned the processed reads to the Mus musculus (mm10) using HISAT v2.1.0 [36]. HISAT utilizes two types of indexes for alignment (a global, whole-genome index and tens of thousands of small local indexes). These two types' indexes are constructed using the same BWT (Burrows–Wheeler transform) a graph FM index (GFM) as Bowtie2. Because of its use of these efficient data structures and algorithms, HISAT generates spliced alignments several times faster than Bowtie and BWA widely used. The reference genome

sequence of Mus musculus (mm10) and annotation data were downloaded from the NCBI.

Transcript assembly and abundance estimation using StringTie [37, 38]. After alignment, StringTie v1.3.4b was used to assemble aligned reads into transcripts and to estimate their abundance. It provides the relative abundance estimates as Read Count of transcript and gene expressed in each sample.

12. Statistical analysis of gene expression level

Expression profile quantified by the HISAT-Stringtie pipeline is used to analyze differentially expressed genes between comparable samples. In the data preprocessing step, genes with one more than zeroed read count values in the samples were excluded. Filtered data were log2-transformed and subjected to TMM Normalization. Statistical significance of the differential expression data was determined using edgeR exactTest [39] and fold change in which the null hypothesis was that no difference exists among groups. False discovery rate (FDR) was controlled by adjusting p-value using Benjamini-Hochberg algorithm. For DE genes which are satisfied with |fold change|≥2 and raw p <0.05, hierarchical clustering analysis was performed using complete linkage method and Euclidean distance as a measure of similarity. Gene-

enrichment and functional annotation analysis and pathway analysis for significant gene list were performed based on gProfiler (https://biit.cs.ut.ee/gprofiler/orth), and KEGG pathway database (https://www.genome.jp/kegg/) respectively. All data analysis and visualization of differentially expressed genes was conducted using R 3.6.0 (www.r-project.org).

13. Data analysis

Enrichr (https://maayanlab.cloud/Enrichr/) is a web-based enrichment analysis tool that includes comprehensive resource libraries and visualizes enrichment gene pathways. [40-42]. Gene Set Enrichment Analysis (GSEA) 4.3.2 version was used for gene analysis.

14. Apoptosis in vitro

To measure the effect of IL-15 signaling on apoptosis, Naïve, TM, $Ly6C^+$ and $Ly6C^-$ VM CD8 T cells were isolated using magnetic sorter and the BD FACS Aria^{TM}III Cell sorter and were then cultured with 0, 2, 20ng/ml rhIL-15 for 3d. Apoptosis was assessed using the FITC Annexin V apoptosis Detection Kit with 7-AAD (BioLegend). For analysis, cells were collected and analyzed using the Fortessa X-20.

15. statistical analysis

All data were analyzed by t-test and Mann-Whitney test using the GraphPad Prism software (GraphPad Software, CA, USA). Bar graph indicates the mean ±SD.

RESULTS

Administration of IL-4 and the anti-IL-4 antibody complex provided protection to mice against lethal influenza A infection

Previous studies have demonstrated that the administration of exogenous IL-4 in complex form with IL-4 plus IL-4 antibody (IL-4C) in naive mice leads to the expansion memory-phenotype CD8 T cells [20, 21]. To assess the in vivo effect of IL-4C treatment, mice were intranasally infected with a lethal dose (6×10^3 pfu/mouse) of PR8 influenza virus (Figure 1A). The survival rate of PR8-infected mice was significantly higher in the IL-4C-treated group than in the groups treated with PBS alone or anti-IL-4 antibodies. Notably, administration of IL-4 alone did not provide protection against lethal influenza (Figure 1B). Unlike IL-4C, which has sustained activity in vivo, IL-4 has a short half-life and transient activity [43]. This suggests that the improved survival observed in IL-4C-treated mice reflects the in vivo bioactivity of IL-4.

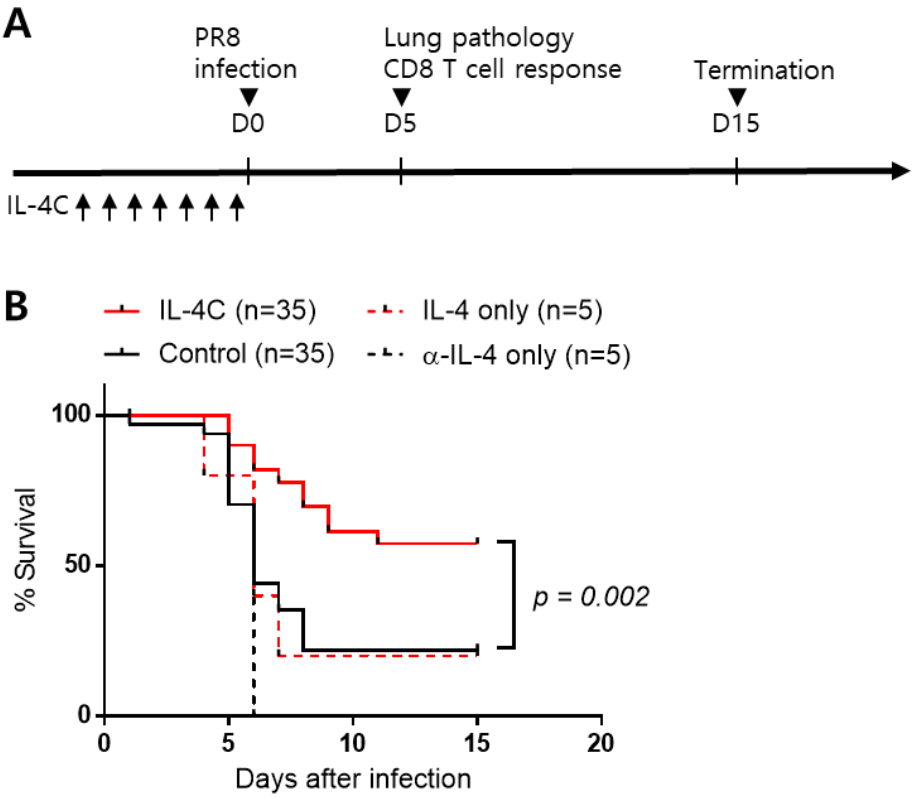

Figure 1. IL-4 and anti-IL-4 antibody complex (IL-4C) treatment protected mice from lethal influenza A virus infection. (A) The experimental protocol. IL-4 (1.5 μg) and anti-IL-4 antibody (7.5 μg) were mixed and administered intraperitoneally to mice daily for 7 days. On day 8, PBS-treated control mice and IL-4C-treated mice were intranasally infected with the PR8 strain of influenza A virus. (B) Survival of influenza-infected mice was monitored daily for 15 days for the following groups: PBS control (n = 35), IL-4C (n = 35), IL-4-only (n = 5), and anti-IL-4 Ab only treated groups (n = 5). Statistical analyses were performed using an unpaired t-test and Mantel-Cox test.

Administration of IL-4C increased accumulation of CD8 T cells in infected lung

Next, the recruitment of total and memory phenotype CD8 T cells was investigated in mice infected with PR8 virus, as these cells play a crucial role in the effective control of the virus. The lungs, lymph nodes, and spleens of infected mice were harvested 5 days post-infection, and the CD8-expressing T cells were analyzed by flow cytometry. It was observed that the lungs of IL-4C-treated mice had more than twice the number of CD8 T cells compared to the control group ($p < 0.01$), while the numbers in the lymph nodes and spleens did not show significant differences (Figure 2A). Furthermore, IL-4C administration increased the number of $CD44^{hi}$ CD8 T cells in all organs (Figure 2B).

Then, it was investigated whether IL-4C could contribute to the expansion of antigen-specific effector/memory CD8 T cell population. CD8 T cells were stained with H2-Db pentamers containing NP366–374 and PA224–233 peptides and it was found that the lungs of IL-4C treated mice had approximately three times more influenza virus-specific CD8 T cells (Figure 2C, 1^{st} graph). Next, to confirm the cytokine-producing function of these CD8 T cells, ex vivo restimulation with influenza NP366–374 peptides performed. The differences in the number of

cytokine-producing cells existed, although they did not reach statistical significance (Figure 2C, 2nd and 3rd graphs)

Previously, it has been reported that not only antigen-specific CD8 T cells but also bystander CD8 T cells, which are cytokine-dependent and TCR-independent, can be activated during pulmonary infection [44]. In the current study, the numbers of both pentamer-negative $CD44^{hi}$ memory-phenotype and $CD44^{low}$ naïve-phenotype CD8 T cells in the lung were also increased by IL-4C treatment, although the increase in $CD44^{low}$ naïve-phenotype CD8 T cells showed marginal significance (Figure 2C, 4th and 5th graphs). Notably, the differences in cell numbers between the IL-4C-treated and control groups were greatest for the pentamer-negative, $CD44^{hi}$ memory-phenotype cell population, which are predominantly bystander memory CD8 T cells. Taken together, these data demonstrated that IL-4C administration enhances the accumulation of both antigen-specific and bystander CD8 T cells in influenza-infected lungs.

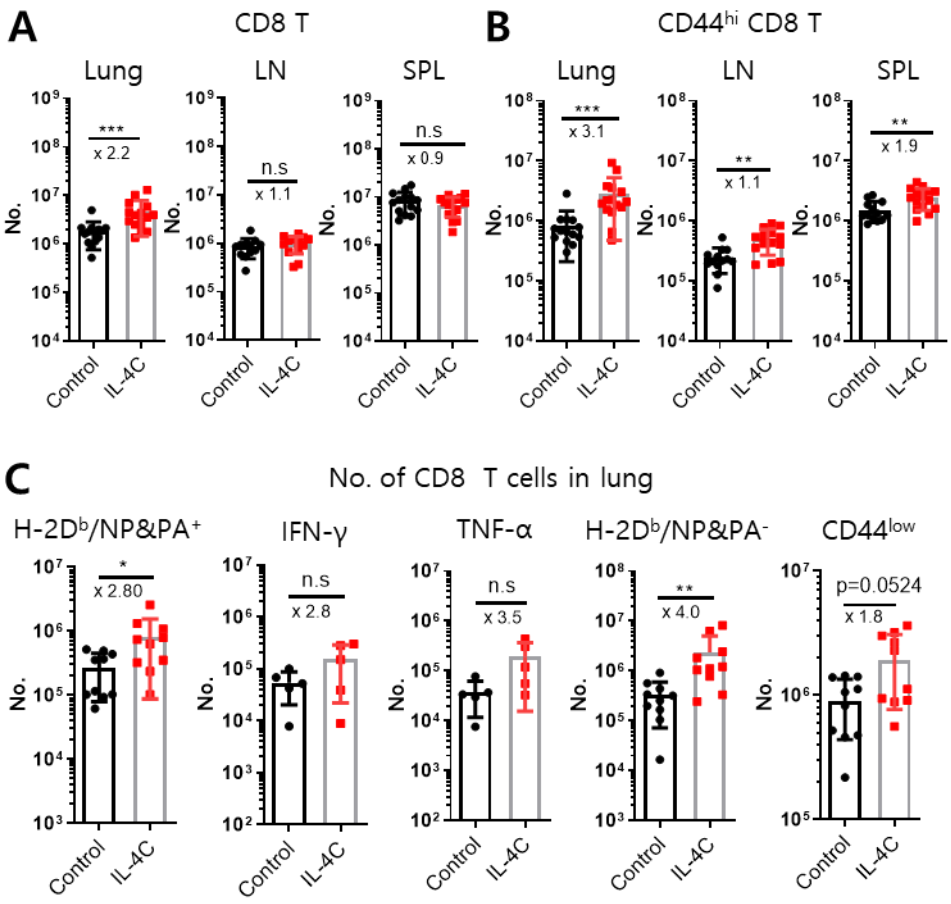

Figure 2. IL-4C treatment enhanced the accumulation of CD8 T cells, influenza-specific and bystander CD8 T cells. Lymphocytes were harvested from the lungs, peribronchial lymph nodes (LNs), and spleen on day 5 post-infection, and CD8 T cells were stained with H-2Db/NP366–374 and H-2Db/PA224–233 pentamers (H-2Db/NP&PA). Lung cells were re-stimulated ex vivo with NP366–374 peptides for 5 hours, and then stained with anti-IFN-γ or TNF-α antibodies and analyzed using flow cytometry. (A-B) The total number of CD8 T cells

(A) and $CD44^{hi}$ memory-phenotype CD8 T cells (B) were quantified. Results are expressed as mean ± SD (n=15/group). (C) The number of antigen-specific (pentamer-, IFN-γ-, or TNF-α-positive) and bystander (pentamer-negative $CD44^{hi}$ or $CD44^{low}$) CD8 T cells was determined by flow cytometry analysis. Data are presented as mean ± SD (n = 5 or 10/group). The x-values represent fold changes. Statistical analysis was performed using an unpaired t-test and Mann-Whitney test. n.s, not significant. *$p < 0.05$; **$p < 0.01$; ***$p < 0.001$

Increased accumulation of CD8 T cells in influenza-infected lungs after IL-4 treatment is dependent on CXCR3

To investigate the underlying mechanism, we focused on the CXCR3 protein. As expected, the proportion of $CXCR3^{+}$ CD8 T cells was higher in IL-4C-treated mice compared to the control group (Figure 3A). To confirm whether CXCR3 expression is involved in the recruitment of T cells, anti-CXCR3-blocking antibodies was injected intraperitoneally into both control and IL-4C-treated mice, followed by intranasal PR8 infection on the same day. On day 5 post-infection, the numbers and phenotypes of CD8 T cells were analyzed. As expected, the treatment with anti-CXCR3 antibodies reduced the effect of IL-4C on the accumulation of both $CD44^{hi}$ and $CD44^{low}$ cells (Figure 3B), indicating that the upregulation of CXCR3 by IL-4C is responsible for the increased accumulation of CD8 T cells. In contrast, the expression of CXCR3 in CD4 cells and their infiltration into infected lungs were not affected by IL-4C and/or anti-CXCR3 antibody (Figure 3C). Furthermore, the transcription of the *Cxcl10* gene, which encodes the major ligand of CXCR3 in influenza-infected lungs, was not affected by IL-4C (Figure 3D), suggesting that IL-4-driven CXCR3 upregulation in $CD44^{hi}$ and $CD44^{low}$ CD8 T cells specifically caused their accumulation in inflamed lungs.

In addition, the influence of IL-4 on other cells involved in the early innate immune response was assessed in control and IL-4C treated mice. The numbers of neutrophils, inflammatory monocytes, and eosinophils did not show significant differences between the IL-4C and control groups on days 1 or 5 after PR8 infection, although the number and frequency of alveolar macrophages was lower in the IL-4C-treated group (Figure 4). Furthermore, the levels of anti-PR8 HA antibodies in the sera of control and IL-4C-treated mice on day 5 after influenza infection were negligible (Figure 5A), suggesting that these antibodies did not contribute to the improved survival of IL-4C-treated mice during the early phase of influenza infection. Similarly, no significant differences in virus titer were observed in the lung (Figure 5B).

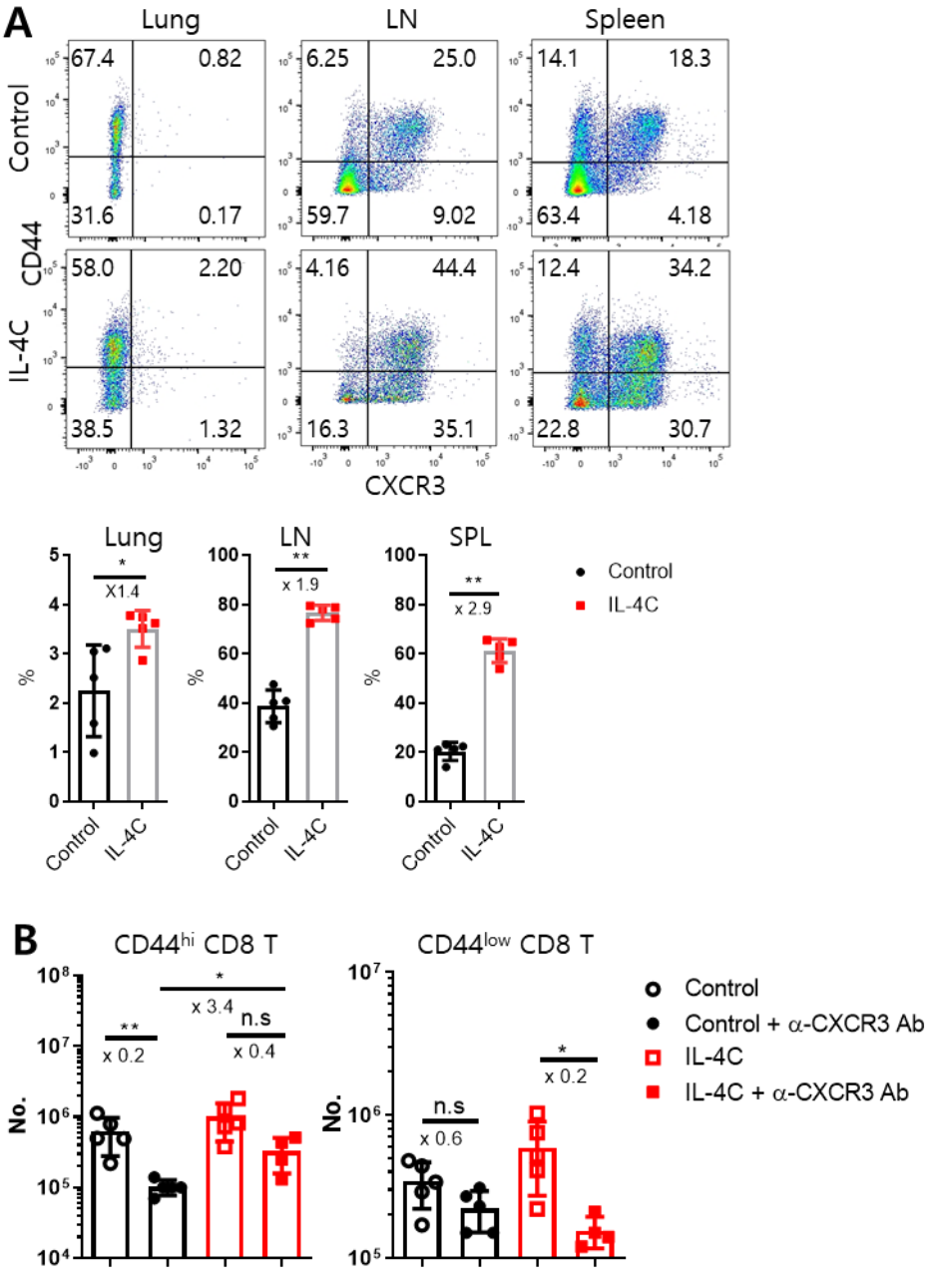
A
Lung
LN
Spleen
Control
IL-4C
CD44
CXCR3
67.4
0.82
31.6
0.17
6.25
25.0
59.7
9.02
14.1
18.3
63.4
4.18
58.0
2.20
38.5
1.32
4.16
44.4
16.3
35.1
12.4
34.2
22.8
30.7
Lung
LN
SPL
%
X1.4
x 1.9
x 2.9
Control
IL-4C
B
CD44hi CD8 T
CD44low CD8 T
No.
x 3.4
n.s
x 0.2
x 0.4
x 0.6
Control
Control + α-CXCR3 Ab
IL-4C
IL-4C + α-CXCR3 Ab

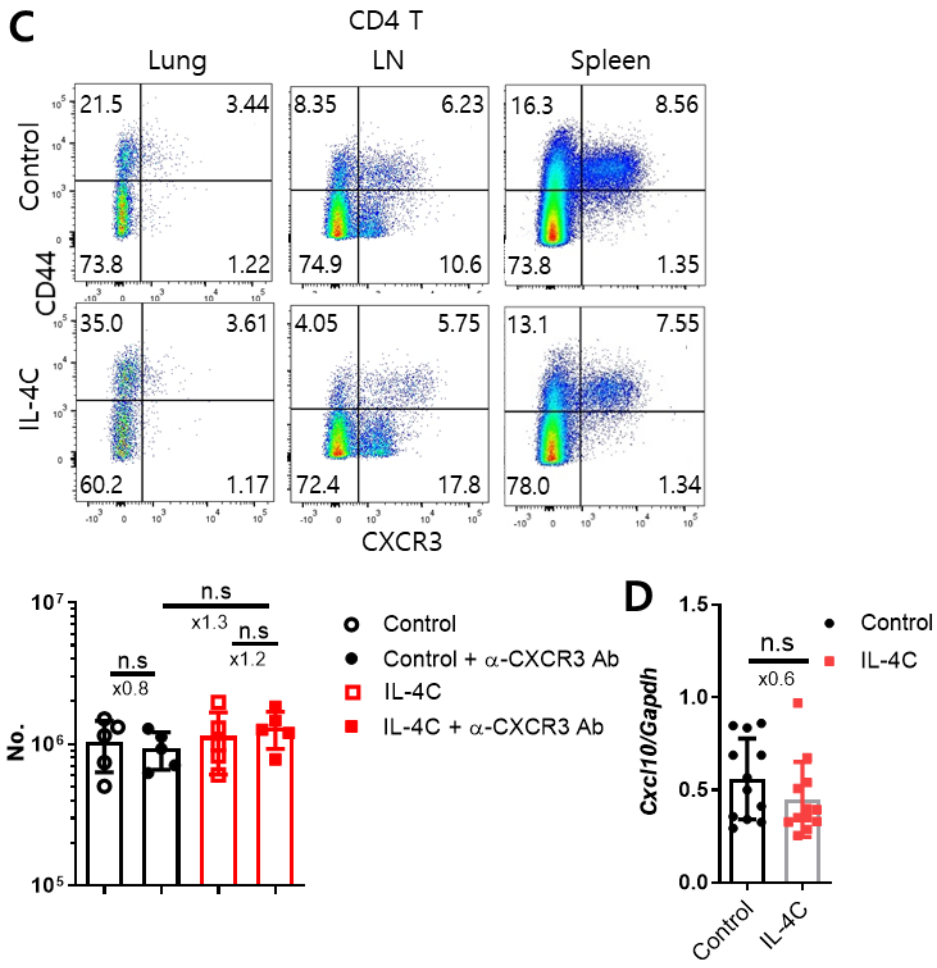

Figure 3. Anti-CXCR3 antibody inhibited IL-4C-induced CD8 T cell accumulation in the lungs. Lymphocytes were harvested from the lungs, peribronchial lymph nodes (LNs), and spleens on day 5 post-infection, and CD8 T cells were analyzed using flow cytometry. (A) The percentage of $CXCR3^{+}$ cells on CD8 cells is shown as a dot plot (upper) and summarized graphs (lower). (B) Mice were treated with IL-4C daily for 7 days, followed by intraperitoneal injection of 500 μg of anti-CXCR3 antibody after influenza A infection. Lung samples were collected 5 days

after infection, and the number of $CD44^{hi}$ and $CD44^{low}$ CD8 T cells was determined by flow cytometry. The results are shown in summarized graphs (n = 5/group). (C) Analysis of CD44 and CXCR3 expression on CD4 T cells from the lung, lymph node (LN), and spleen at day 5 post-infection, as well as the absolute number of CD4 T cells in the lungs of control and IL-4C-treated mice with or without anti-CXCR3 antibody. The representative dot plot and summarized graph are shown (n = 5/group). (D) Measurement of Cxcl10 transcript levels in the lung at 5 days post-infection using real-time PCR. Expression levels were normalized to the Gapdh gene. A summarized graph is shown (n = 10/group). The x-values represent fold change. Statistical analysis was performed using an unpaired t-test and Mann-Whitney test. n.s, not significant. *$p < 0.05$; **$p < 0.01$.

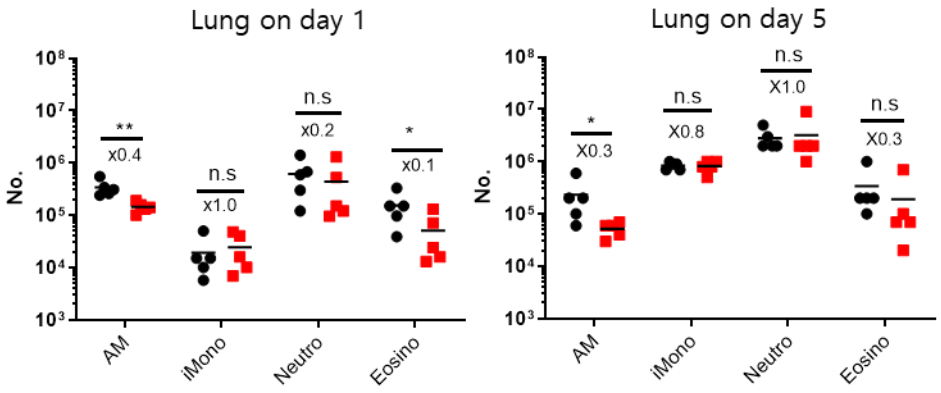

Figure 4. The number of innate immune cells in the lungs was similar between control and IL-4C-treated mice. Cells were isolated from the lungs of control and IL-4C-treated mice on days 1 and 5 after infection. Calculation of the number of innate cells, including alveolar macrophages (AM), inflammatory monocytes (iMono), neutrophils (Neuro) and eosinophils (Eosino), are presented as mean ± SD (n = 12/group). The x-values represent the fold change. Statistical analysis was performed using an unpaired t-test and Mann-Whitney test. n.s, not significant. *$p < 0.05$; **$p < 0.01$.

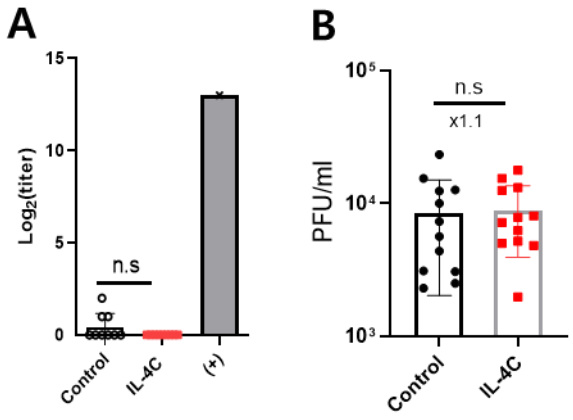

Figure 5. Antibody levels and virus titers in infected mice were not significantly different. Control and IL-4C-treated mice were infected intranasally with PR8 and the groups were sacrificed 5 days after infection. (A) Anti-PR8 HA antibody titers in serum of control and IL-4C-treated mice were measured by ELISA. A summary graph is shown (n = 9/group). (B) Virus titers in the lungs of each group were analyzed by plaque assay. A pooled graph is shown (n = 12/group). The x-values represent fold change. Statistical analysis was performed using an unpaired t-test and Mann-Whitney test. n.s, not significant.

Type I IFN, IL-4, and IL-15 exert distinct effects on different subsets of VM CD8 T cells.

The discovery that the administration of exogenous IL-4 significantly reduced the mortality rate of influenza-infected mice and enhanced the infiltration of CD8 T cells into the infected lungs prompted further investigation. I further investigated whether VM cells induced by cytokines such as IL-4, type I IFN and IL-15 are a homogeneous or heterogeneous population. Although certain markers such as CXCR3, CD122, and Eomes are known to be expressed by VM CD8 T cells, they do not distinguish between IL-4, type I IFN, and IL-15-dependent VM CD8 T cells [4]. Therefore, in this study, two molecules, Ly6C and Sca-1, which are known to be upregulated by type I IFN [23, 24], were used to identify type I IFN-dependent VM cells. Subsequently, CD8 T cell subsets from WT and IFNAR1 KO mice, lacking the receptor for both IFN-α and IFN-β, were compared. Flow cytometry revealed no significant difference in the total number of CD8 T cells and $CD44^{hi}$ $CD49d^{-}$ VM CD8 T cells in the spleens of WT C57BL/6 mice and IFNAR1 KO mice (Figure 6A). VM CD8 T cells were further categorized into four subsets based on Ly6C and Sca-1 expression: $Ly6C^{+}Sca\text{-}1^{-}$ (Q1), $Ly6C^{+}Sca\text{-}1^{+}$ (Q2), $Ly6C^{-}Sca\text{-}1^{+}$ (Q3), and $Ly6C^{-}Sca\text{-}1^{-}$ (Q4). $Ly6C^{+}Sca\text{-}1^{-}$ (Q1) and $Ly6C^{+}Sca\text{-}1^{+}$ (Q2) cells were the two major populations in WT mice. Notably, the frequency and number of

Sca-1$^+$ (either Ly6C$^+$ or Ly6C$^-$) VM CD8 T cells were significantly reduced in IFNAR1 KO mice, particularly in the Ly6C$^+$Sca-1$^+$ (Q2) subset (25-fold reduction) compared with Ly6C$^-$Sca-1$^+$ (Q3) cells (5-fold reduction) (Figure 6B and C). Conversely, the number of Ly6C$^-$Sca-1$^-$ (Q4) cells was increased, and the Ly6C$^+$Sca-1$^-$ (Q1) fraction remained unaffected by IFNAR1 deficiency (Figure 6C).

Next, to investigate whether IL-4 was also involved in the generation of the similar or different subsets of VM CD8 T cells, the subsets of VM CD8 T cells in WT control and IL-4 KO mice were compared. Total number of splenocytes and VM CD8 T cells was slightly decreased in the IL-4 KO mice compared with the WT mice (Figure 7A). Subset analysis of VM cells revealed an approximately 3-fold reduction in the number of Ly6C$^+$ Sca-1$^-$ (Q1) cells in IL-4 KO mice (Figure 7B and C). These results clearly demonstrate that IL-4 and type I IFN signaling induce the development of a distinct subset of VM CD8 T cells. Specifically, the absence of IL-4 affected the Ly6C$^+$ Sca-1$^-$ (Q1) VM CD8 T cells, whereas the absence of type I IFN signaling impacted the Ly6C$^+$ Sca-1$^+$ (Q2) and Ly6C$^-$ Sca-1$^+$ (Q3) VM CD8 T cells.

IL-15 is well known for its role in enhancing the proliferation and survival of memory phenotype CD8 T cells [45]. In addition, IL-15 is crucial for the development of NKT cells, which are prototypic innate T

cells, and IL-4-induced innate CD8 T cells [1]. Therefore, it is reasonable to speculate that IL-15 may also be required for the development of IL-4 and type I IFN-dependent VM CD8 T cells. To investigate this hypothesis, VM CD8 T cell subsets were compared between WT and IL-15Ra KO mice. As expected, flow cytometric analysis of splenocytes from these mice revealed a significant decrease in both the absolute number and percentage of VM CD8 T cells in the IL-15Ra KO mice (Figure 8A). Subset analysis of the VM cells further demonstrated significant reduction in $Ly6C^{+}$ $Sca\text{-}1^{-}$ VM (Q1, 25-fold reduction) and $Ly6C^{+}$ $Sca\text{-}1^{+}$ VM (Q2, 3-fold reduction) subsets (Figure 8B and C). These results provide evidence supporting the notion that IL-15 is required for the development and/or maintenance of $Ly6C^{+}$ VM CD8 T cells.

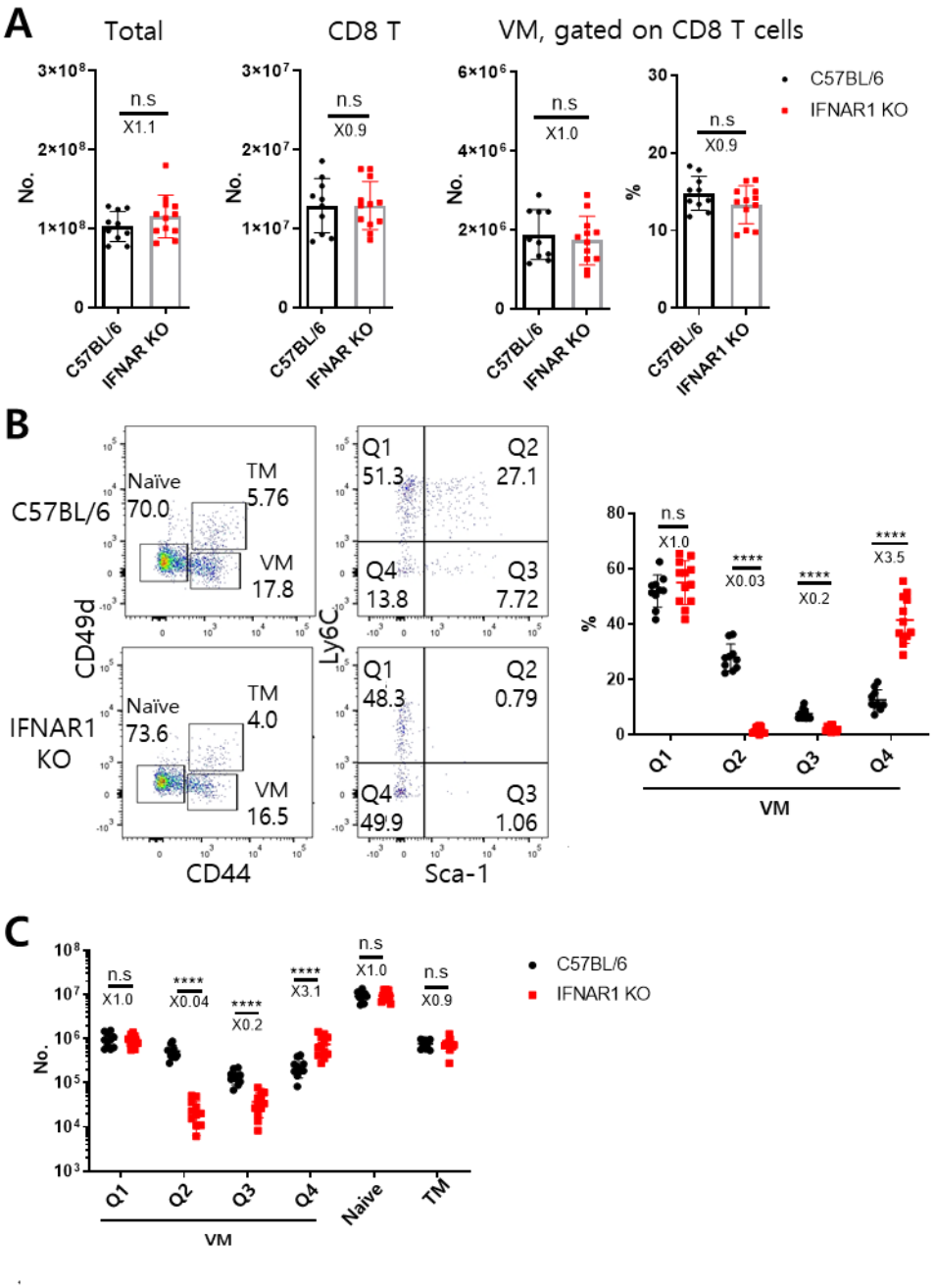

Figure 6. Development of Sca-1^{+} VM CD8 T cells is dependent on type I IFN signaling. Splenocytes from wild-type (WT) C57BL/6 and IFNAR1 KO mice were analyzed by flow cytometry. (A) Summarized

graphs showing the absolute numbers and frequencies of total splenocytes, CD8 T cells and virtual memory CD8 T cells. (B) Representative dot plots illustrate the frequency of the different subsets of CD8 T cells, including naive, VM and TM populations (left) and the subsets within VM cells (right). The frequency of VM subsets is presented as a graph. (C) The summarized graph displays the absolute number of each CD8 T cell subset. The numbers within the plots indicate the percentage of cells within each rectangle or quadrant. Summarized data (n=10~12/group) are presented as mean ± SD with the fold changes between the two groups indicated by the x-numbers. Statistical analyses were performed using an unpaired t-test and Mann-Whitney test. n.s, not significant. ****$p < 0.0001$.

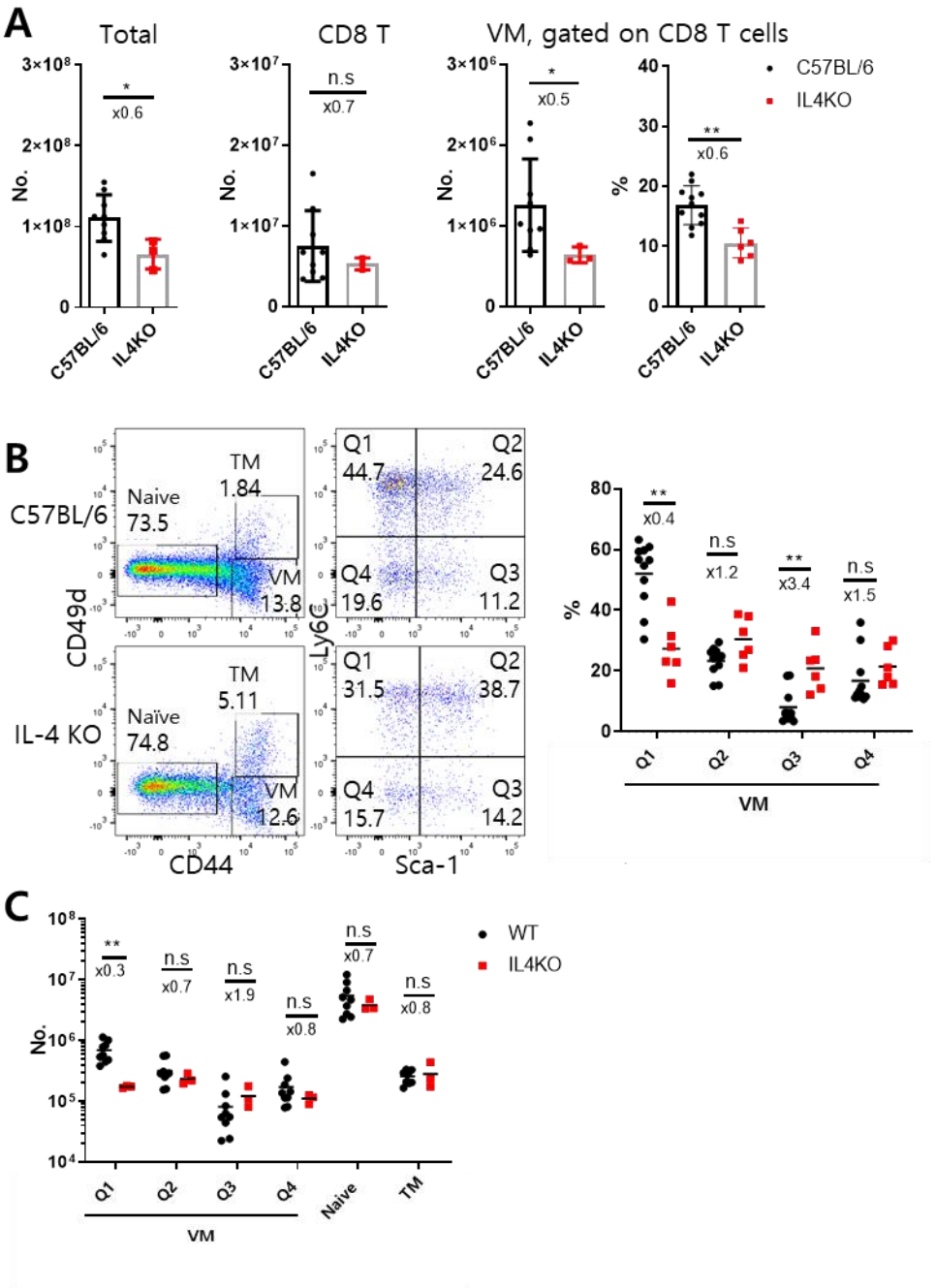

Figure 7. Development of Ly6C^{+} Sca-1^{-} VM cells was partially defective IL-4 mice. Splenocytes were collected from both C57BL/6

and IL-4 KO mice and stained for CD44, CD49d, Ly6C, and Sca-1. (A) The summarized graph shows the total number of splenocytes, CD8 T cells, and VM CD8 T cells, as well as the percentage of VM CD8 T cells among the total CD8 T cells in both C57BL/6 WT and IL-4 KO mice. (B) Representative dot plots illustrate the frequency of the different subsets of CD8 T cells, including naive, VM and TM populations (left) and the subsets within VM cells (right). The frequency of VM subsets is presented as a graph. (C) The summarized graph displays the absolute number of each CD8 T cell subset. The numbers within the plots indicate the percentage of cells within each rectangle or quadrant. Summarized data (n=3~9/group) are presented as mean ± SD with the fold changes between the two groups indicated by the x-numbers. Statistical analyses were performed using an unpaired t-test and Mann-Whitney test. n.s, not significant. *$p < 0.05$. **$p < 0.001$.

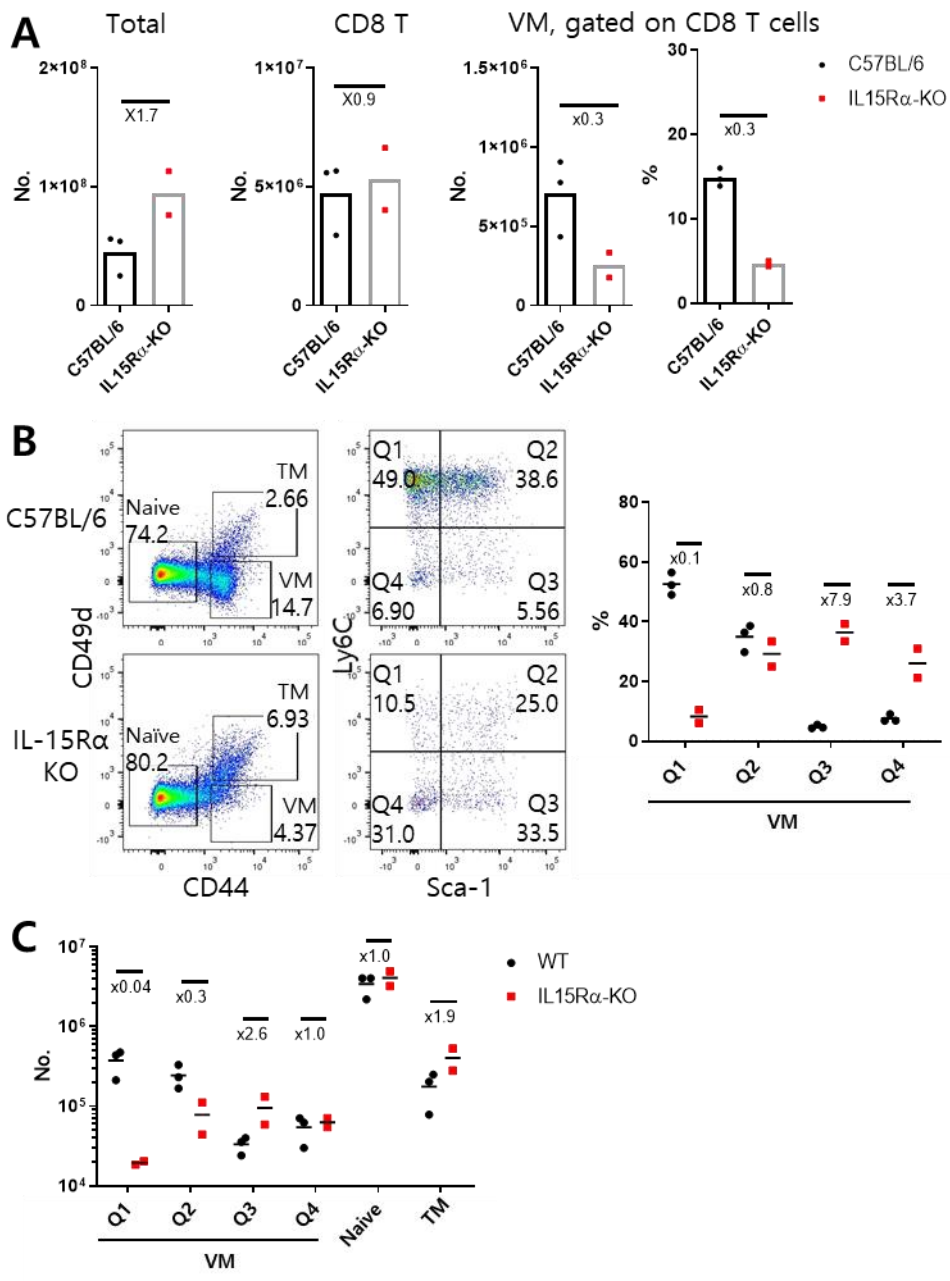

Figure 8. Ly6C^{+} VM CD8 T cells are susceptible to IL-15 signaling.

Splenocyte were obtained from C57BL/6 and IL-15Rα KO mice and analyzed by flow cytometry. (A) The absolute number and percentage of

total splenocytes, CD8 T cells and VM CD8 T cells were summarized as a graph. (B) Representative dot plots illustrate the frequency of the different subsets of CD8 T cells, including naive, VM and TM populations (left) and the subsets within VM cells (right). The frequency of VM subsets is presented as a graph. (C) The summarized graph shows the absolute number of each CD8 T cell subset. The numbers within the plots indicate the percentage of cells within each rectangle or quadrant. Summarized data (n=2-3/group) are presented as mean ± SD with the fold changes between the two groups indicated by the x-numbers.

Ly6C$^+$ and Ly6C$^-$ VM CD8 T cells exhibit distinct gene expression patterns

To gain insight into the molecular characteristics of VM CD8 T cell subsets based on Ly6C and Sca-1 expression, different populations including naïve (CD44$^{-/low}$), TM (CD44^{hi} CD49d$^+$), and specific subpopulations of VM (CD44^{hi} CD49d$^-$) CD8 T cells were isolated from the spleens of WT mice using magnetic and flow cytometric sorting. The isolated cells were then subjected to bulk mRNA sequencing (RNA-Seq) analysis (Figure 9A). Initially, a total of 3,431 differentially expressed genes (DEGs) were identified using a filter based on a p-value of less than 0.05 and a fold change greater than 2. These DEGs were further analyzed via principal component analysis (PCA) to elucidate the relationships between the different T cell populations (Figure 9B). The PCA plot clearly demonstrated the separation of the Ly6C$^+$ VM subsets (Q1 and Q2) from the Ly6C$^-$ VM fractions (Q3 and Q4). TM cells showed a certain degree of proximity to the Ly6C$^-$Sca-1$^+$ (Q3) VM subset, while naïve cells displayed a close relationship with the Ly6C$^+$ Q1 and Q2 subsets in the first principal component (P1), although they remained distinct from both the VM and TM populations. These findings strongly suggest that the Ly6C$^+$ and Ly6C$^-$ VM subsets represent distinct populations characterized by unique gene expression profiles.

To investigate the factors contributing to these differences, the gene expression profiles of naïve and TM CD8 T cells were compared. A total of 1,874 DEGs were identified from the initial set of 3,431 genes, using a filter based on a p-value less than 0.05 and a fold change greater than 2. Pathway analysis using Bioplanet 2019 (p-value ranking) in Enrichr (https://maayanlab.cloud/Enrichr/) yielded the top 10 pathways enriched in naïve or TM cells (Figure 9C). The majority of pathways upregulated in TM vs naïve cells were related to the cell cycle (Table 1). Among these pathways, the *Polo-like kinase (PLK) pathway* is associated with critical stages of the cell cycle and supports cell division [46]; the *Aurora B signaling pathway* induces chromosome segregation [47]; and *the E2F transcription factor* is a key regulator of G1-to-S phase transition in the cell cycle [48]. The heatmap analysis of DEGs in cell cycle related gene signatures revealed a close relationship between naïve and $Ly6C^+$ subsets, as well as a relationship between TM and $Ly6C^-$ VM CD8 T cells (Figure 10A).

Another notable pathway was the *IL-2 signaling pathway*, which can be divided into two clusters (Figure 10B, Table 2). Group 1 genes were upregulated in both $Ly6C^+$ VM subsets and TM cells compared with naïve and $Ly6C^-$ VM cells. This group included VM-related genes, such as *Eomes, Cxcr3, Il2rb* (encoding CD122, IL-2/IL-15Rα common for IL-2 and IL-15), and *Ccr5*. Of particular interest, the *Cxcr3* and *Ccr5*

genes have been reported to be upregulated in IL-15-induced bystander-activated CD8 T cells; they play a crucial role in the recruitment of CD8 T cells to the lung [49, 50]. In contrast, group 2 genes were upregulated in Ly6C$^-$ VM subsets and TM cells. This group included *Il2ra* (encoding CD25, the IL-2 receptor specific to IL-2), *Bcl6*, *Ccnd1* (encoding cyclin D1), and *Cx3cr1*. *Bcl6* plays an important role in regulating the development and maintenance of antigen-specific memory CD8 T cells [51].

The tenth enriched pathway in the comparison between TM and naïve CD8 T cells was the *selective expression of chemokine receptors during T-cell polarization* (Figure 10C). Some of the chemokine genes included in this pathway overlapped with genes in the *IL-2 signaling pathway* (Table 2). Heatmap analysis of the chemokine genes in this pathway revealed distinct expression patterns, including *Ccr7* and *Cxcr5*, which encode lymph node homing receptors, and *Cxcr4*, which encodes a bone marrow homing receptor (Figure 10C) [52].

As shown in Figure 9C, the pathway analysis also revealed the top 10 pathways upregulated in naïve vs TM cells, which include the *cyanoamino acid metabolism*, the *taurine and hypotaurine metabolism*, and the *osteoblast signaling*. However, these pathways lacked adequate number of DEGs to draw meaningful conclusions (Table 3).

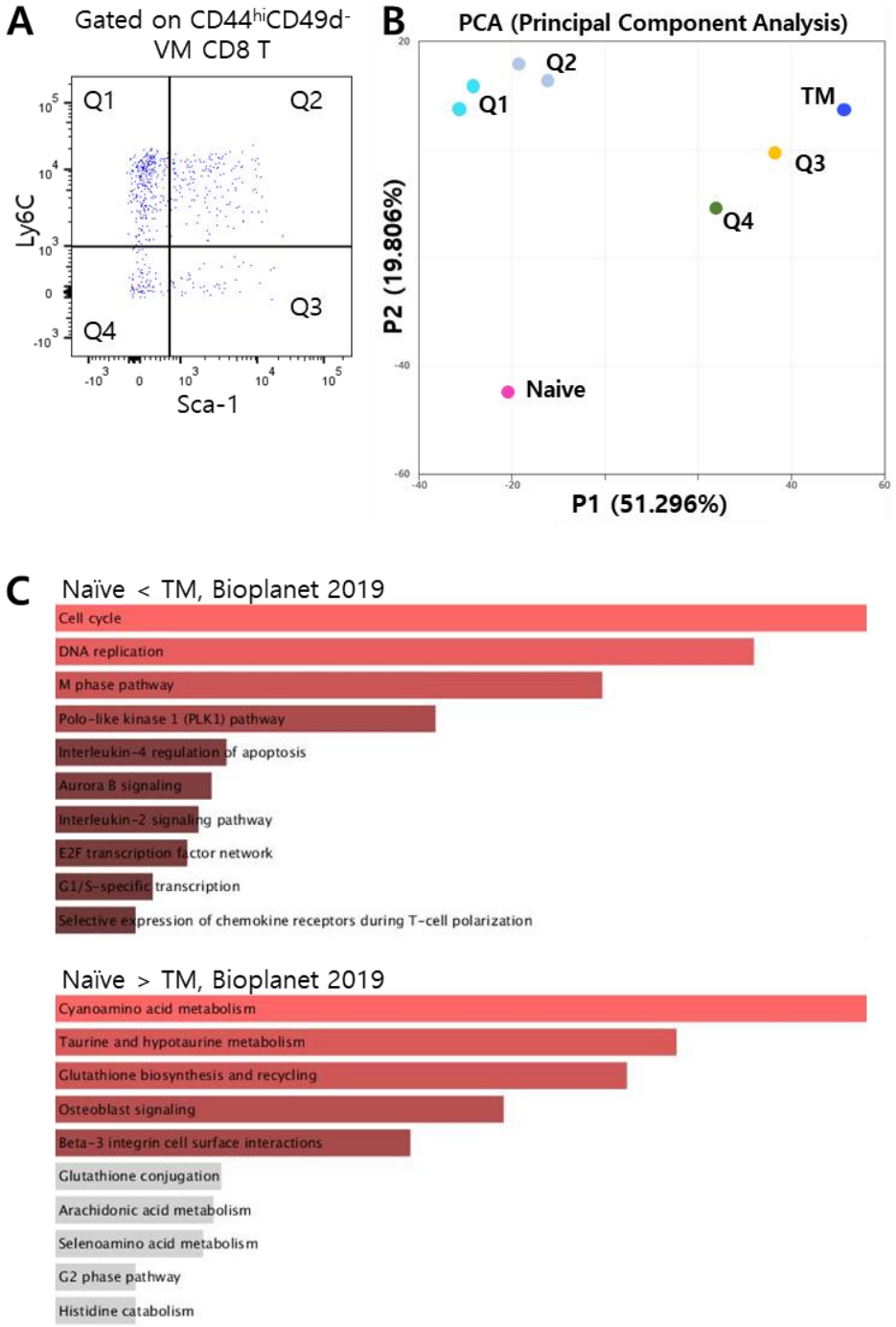

Figure 9. RNA-Seq analysis results reveal the relationship between CD8 T cell subsets and the top 10 enriched pathways in TM and

naïve CD8 T cells. CD8 T cells were isolated from the spleen of C57BL/6 mice using MACS and FACS AriaTMIII, followed by bulk mRNA sequencing. (A) Gating strategy for RNA-Seq analysis of $CD44^{hi}CD49d^{-}$ VM CD8 T cell subsets. (B) Differential expression analysis using RNA-Seq data revealed a total of 3,431 genes that showed significant changes between VM CD8 T cells, naïve cells, and TM cells. The results were visualized using a PCA plot (p-value < 0.05, fold-change > 2). (C) The top 10 enriched pathways between naïve and TM cells were analyzed using the Enrichr website. The bar graph shows the ranking of these pathways based on their p-values, with the most significant pathways displayed. The analysis was performed using bioplanet 2019, and the brightness of the color indicates the level of significance associated with each pathway

Table 1. Upregulated DEGs in TM vs naïve CD8 T cells

	Name	P-value	Adjusted P-value	Odds Ratio	Combined Score	Genes
1	Cell cycle	2.37E-18	2.67E-15	3.175472	128.8772	TOP2A;CDKN1A;FEN1;ERCC6L;MCM8;ZWILCH;GMNN;BUB1B;MCM10;BRCA1;CKS1B;LMNB1;CDC20;CCND1;CDH1;MIS18BP1;NUF2;CHEK1;NEK2;OIP5;KNTC1;MYBL2;SPDL1;NINL;POLE;RFC3;RFC4;LIG1;H2AFZ;H2AFX;TBC1D8;KIF23;MPEG1;CDC25B;CCNA2;TFDP1;ESPL1;CCNE2;INCENP;MCM3;BIRC5;MCM5;KIF2C;DNA2;KIF20A;CDCA8;TTK;TYMS;CENPA;SKA1;NSL1;AURKB;SKA2;AURKA;CCNB2;SYCE2;CCNB1;CDC45;ORC1;PRKAR2B;LMNA;E2F1;E2F2;E2F3;CLSPN;BUB1;PLK4;GINS1;GINS2;CDKN2C;RRM2;TGFB3;UBE2C;PLK1;CDC6;NDC80;DHFR;CENPE;POLA1;CENPF;KIF18A;WEE1;CENPH;CENPI;ALMS1;CENPK;CENPL;CDK1;CENPM;CENPN;CENPP;SPC24;MAD2L1;SPC25
2	DNA replication	1.15E-16	6.47E-14	4.436245	162.8341	CDKN1A;FEN1;ERCC6L;ZWILCH;MCM8;GMNN;BUB1B;MCM10;CDC20;NUF2;KNTC1;SPDL1;POLE;RFC3;RFC4;LIG1;KIF23;CCNA2;INCENP;MCM3;BIRC5;KIF2C;MCM5;DNA2;KIF20A;CDCA8;CENPA;SKA1;AURKB;NSL1;SKA2;CDC45

						;ORC1;E2F1;E2F2;E2F3;BUB1;GINS1;GINS2;PLK1;CDC6;NDC80;POLA1;CENPE;CENPF;KIF18A;CENPH;CENPI;CENPK;CENPL;CENPM;CENPN;CENPP;SPC24;MAD2L1;SPC25
3	M phase pathway	2.11E-14	7.94E-12	6.498157	204.6218	ERCC6L;ZWILCH;BUB1B;CDCA8;CENPA;AURKB;NSL1;SKA1;SKA2;CDC20;NUF2;KNTC1;SPDL1;BUB1;PLK1;KIF23;NDC80;CENPE;CENPF;KIF18A;CENPH;INCENP;CENPI;CENPK;CENPL;BIRC5;CENPM;KIF2C;CENPN;KIF20A;CENPP;SPC24;MAD2L1;SPC25
4	Polo-like kinase 1 (PLK1) pathway	6.53E-12	1.84E-09	9.890704	254.7325	ERCC6L;PLK1;BUB1B;NDC80;AURKA;CDC25B;CDC20;CENPE;TPX2;CCNB1;PAK1;WEE1;INCENP;PRC1;CDK1;CLSPN;KIF20A;ECT2;BUB1;NINL;SPC24
5	Interleukin-4 regulation of apoptosis	8.61E-09	1.94E-06	2.735518	50.7989	TOP2A;CD86;SUV39H2;CDKN1A;ITGAM;UBE2L6;LITAF;RGS2;CYSLTR2;CASP3;TMOD1;ANXA1;FCER1G;DST;ITGA2;GEM;VCAN;MAF;KIT;MCM3;XCL1;MCM5;TLR4;CHST2;NDRG4;PTGER2;GCNT1;FGL2;PDGFB;LPL;CSF2RB;NUAK1;ATXN1;CDC45;NFIL3;COBLL1;JAG1;VCAM1;IL10RA;GZMA;MX1;GZMB;GCSAM;ELL2;ARHGAP32;BCL6;POU2AF1;ALOX5AP;CD9;MAD2L1

6	Aurora B signaling	1.44E-08	2.70E-06	8.165811	147.4574	CDCA8;NCAPG;KIF23;CENPA;AURKB;NCAPH;NDC80;AURKA;SMC2;INCENP;STMN1;BIRC5;KIF2C;NCAPD2;KIF20A;BUB1
7	Interleukin-2 signaling pathway	2.26E-08	3.64E-06	1.851915	32.60411	CSF1;INPPL1;RORA;AHR;LAPTM4B;IL18RAP;CCND1;RGS1;MYB;EOMES;CD300A;FRMD4B;PASK;CDC25B;RAB31;S100A4;ADAM8;GPLD1;CSF2RB;CSF2RA;SOCS2;GRK5;PMAIP1;CLSPN;KLRC1;S100A11;LYN;FUCA1;GPR137B;NR4A2;BCL6;BHLHE40;CDK1;PLXNB2;PKIG;EZH2;BCL2L1;DOCK5;ITGAM;CTSZ;PLEK;PIK3CB;LITAF;CASP3;ITGAX;CASP1;CTSH;CCR5;DUSP4;DUSP5;DUSP3;FCER1G;SYK;TBC1D8;GAB2;KIF22;DUSP9;FGR;ZEB2;CEACAM1;SLC7A7;MDFIC;IFNG;IRF4;IL1B;XCL1;IRF5;MAPRE2;TLR4;CX3CR1;HEMGN;CLDND1;AHNAK;SRC;PTGER2;RGS16;CXCR5;TTK;AIF1;PAK1;NFIL3;CHSY1;CAMK2N1;CCL5;SPOCK2;CXCR3;CCL4;CCL3;HSF4;CTNNA1;E2F2;E2F3;IL12RB1;IL12RB2;GALNT3;GZMA;MX1;CARD9;GZMB;VEGFA;GZMM;GALE;EVI2A;CD40LG;THEMIS2;CENPI;PSAT1;IL2RA;IL2RB;YPEL1;CD68;MYO1F;PTPN3

8	E2F transcription factor network	3.32E-08	4.68E-06	4.977455	85.71885	CDKN1A;RRM1;CDKN2C;RRM2;BRCA1;CDC6;TYMS;HIC1;CCNA2;POLA1;TFDP1;CCNE2;ORC1;MCM3;E2F1;RBBP8;CDK1;E2F2;MYBL2;E2F3;TK1;E2F7
9	G1/S-specific transcription	1.09E-07	1.37E-05	16.71964	268.0752	DHFR;POLA1;RRM2;CDC45;TFDP1;ORC1;CDK1;E2F1;CDC6;TYMS
10	Selective expression of chemokine receptors during T-cell polarization	1.96E-07	2.22E-05	10.04074	155.0652	CD4;CD40LG;IFNG;TGFB3;CXCR3;CCL4;CCL3;CCR5;IL12RB1;CCR4;CCR3;IL12RB2

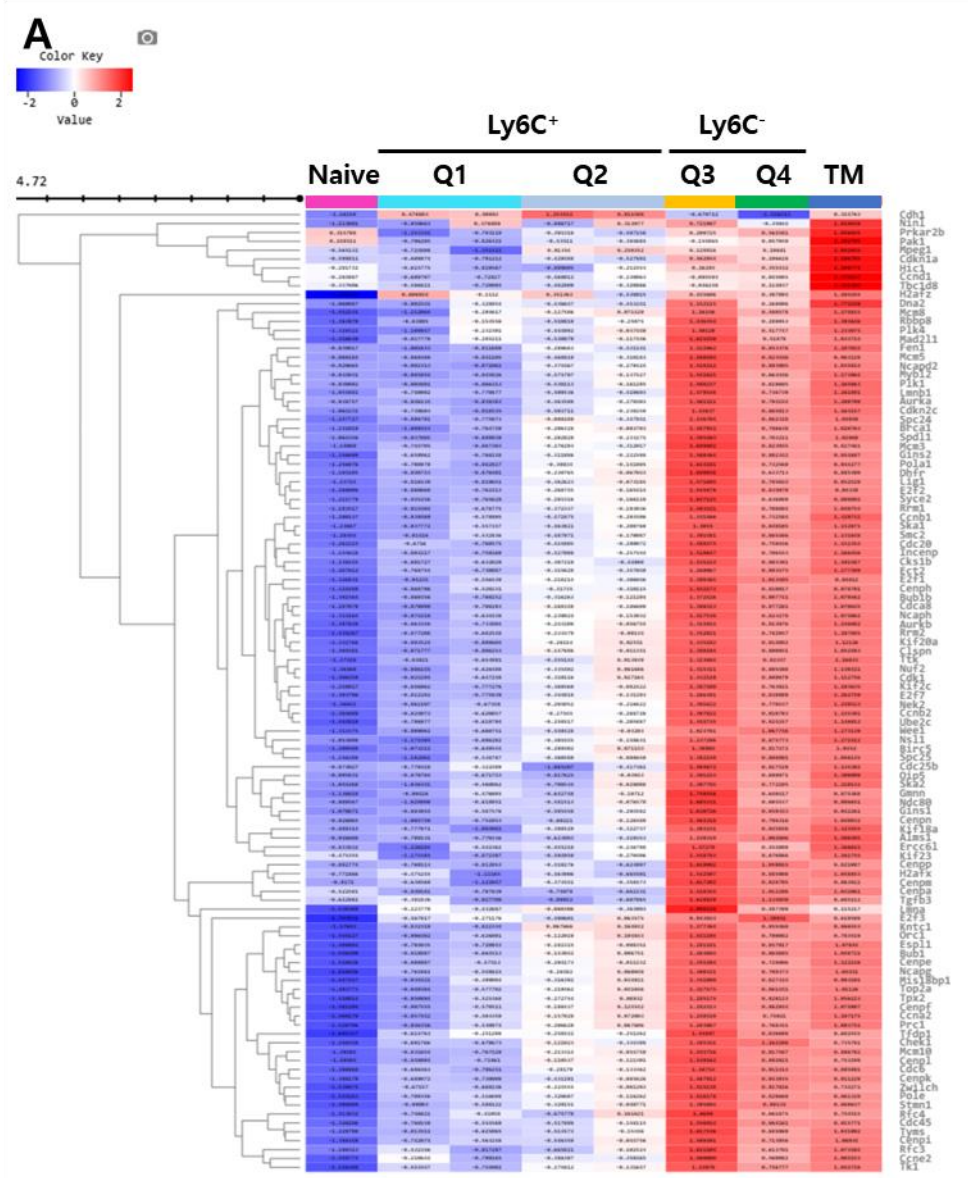
A
Color Key
-2
0
2
Value
4.72
Ly6C+
Ly6C-
Naive
Q1
Q2
Q3
Q4
TM
Cdh1
Nin1
Prkar2b
Pak1
Mpeg1
Cdkn1a
Hic1
Ccnd1
Tbc1d8
Hzaf2
Dna2
Mcm8
Rbbp8
Plk4
Mad2l1
Fen1
Mcm6
Ncapd2
Myb12
Plk1
Tnpb1
Aurka
Cdkn2c
Spc24
Brca1
Spdl1
Mcm3
Gins2
Pola1
Dbfr
Lig1
E2f2
Syce2
Rrm1
Ccnb1
Ska1
Smc2
Cdc20
Incenp
Cks1b
Esco2
E2f1
Cenph
Bub1b
Cdca8
Ncaph
Aurkb
Rrm2
Klf20a
Ctcfl
Tk1
Nuf2
Cdk1
Klf2c
E2f7
Wee2
Ccnb2
Ube2c
Wee1
Nsl1
Birc5
Spc25
Cdc25b
Klf23
Cenpp
Ska2
Gmnn
Ndc80
Gins1
Cenpn
Klf18a
Alms1
Ercc6l
Klf23
Cenpp
H2afx
Cenpe
Cenpa
Tgfb3
Lmnb1
E2f3
Kntc1
Orc1
Espl1
Bub1
Cenpe
Ncapg
Mis18bp1
Top2a
Tpx2
Cenpf
Ccna2
Prc1
Tfdp1
Chek1
Mcm10
Cenpl
Cdc6
Cenpk
Zw1ch
Pole
Stmn1
Rfc4
Cdc45
Tyms
Cenpi
Rfc3
Ccne2
Tk1

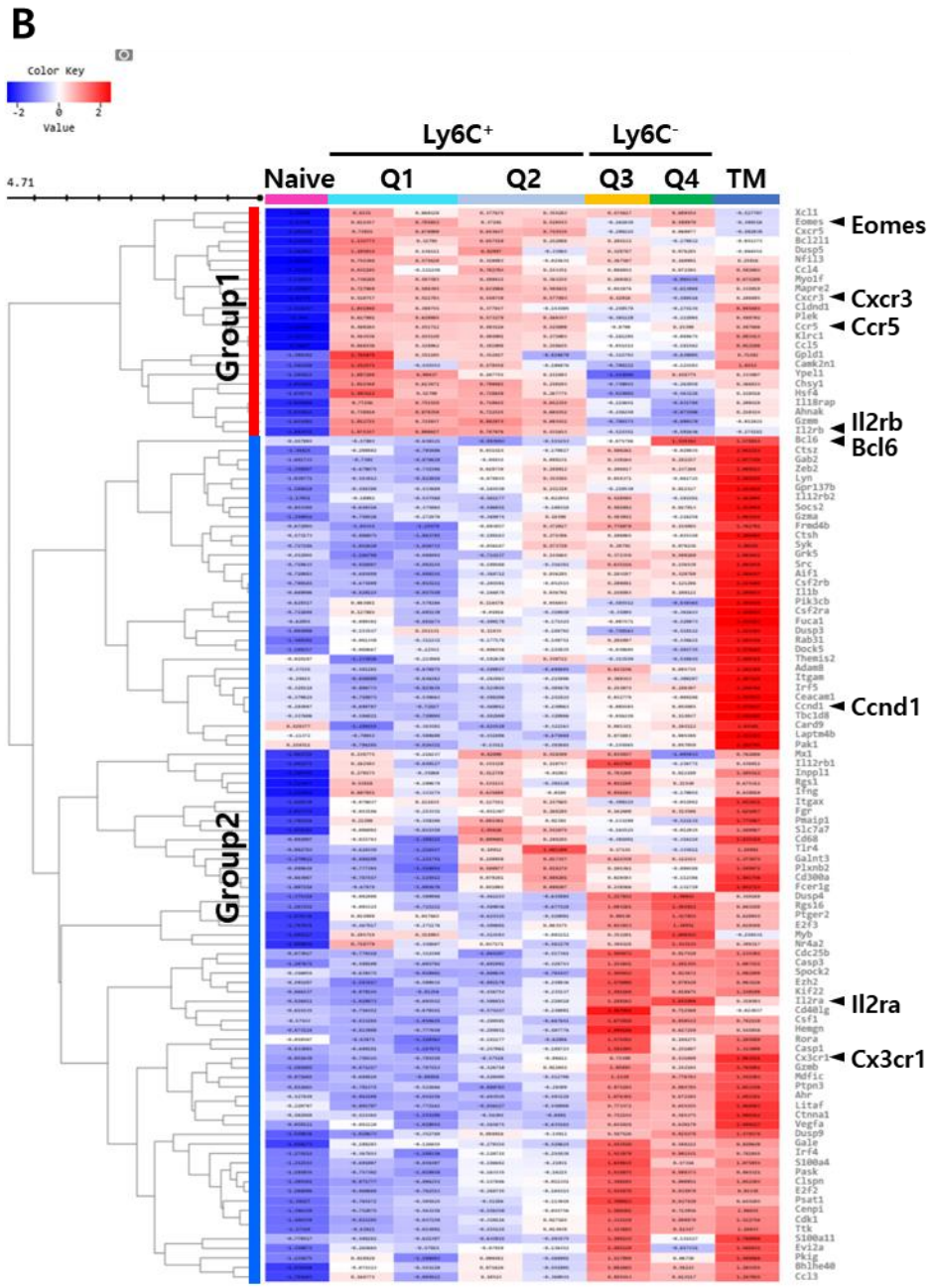
B
Color Key
-2
0
2
Value
4.71
Ly6C+
Ly6C-
Naive
Q1
Q2
Q3
Q4
TM
Group1
Group2
Eomes
Cxcr3
Ccr5
Il2rb
Bcl6
Ccnd1
Il2ra
Cx3cr1

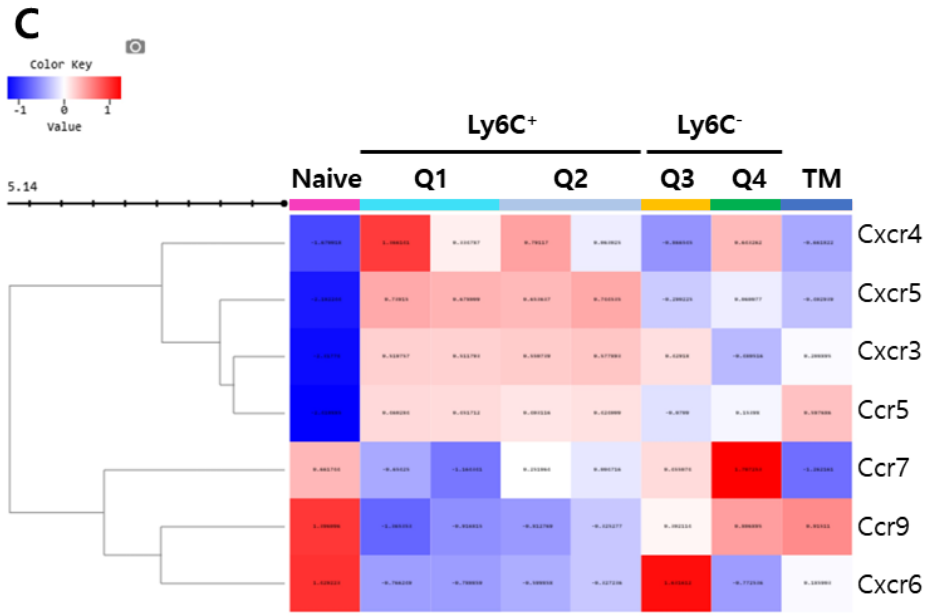

Figure 10. DEGs of top 10 upregulated pathways in TM vs naïve CD8 T cells were compared across the all subsets of CD8 T cells. (A) A heatmap analysis was performed on cell cycle related genes, namely Cell cycle, DNA replication, M phase pathway, PLK1 pathway, Aurora B signaling, and E2F transcription factor network, which were identified as part of the top 10 enriched pathways upregulated in TM cells. The resulting heatmap highlights differences in gene expression patterns between the $Ly6C^+$ and $Ly6C^-$ VM subsets, indicating their similarity to naïve or TM cells, respectively. (B) The DEGs of the interleukin-2 signaling pathway categorized into two groups based on their expression patterns in the $Ly6C^+$ and $Ly6C^-$ VM subsets by heatmap analysis. (C) A heatmap was generated to visualize the differential expression patterns of chemokine receptors in all subsets of CD8 T cells.

Table 2. Interleukin-2 signaling pathway

	Genes
Group 1	Xcl1, Eomes, Cxcr5, Bcl2l1, Dusp5, Nfil3, Ccl4, Myo1f, Mapre2, Cxcr3, Cldnd1, Plek, Ccr5, Klrc1, Ccl5, Gpld1, Camk2n1, Ypel1, Chsy1, Hsf4, Il18rap, Ahnak, Gzmm, Il2rb
Group 2	Bcl6, Ctsz, Gab2, Zeb2, Lyn, Gpr137b, Il12rb2, Socs2, Gzma, Frmd4b, Ctsh, Syk, Grk5, Src, Aif1, Csf2rb, Il1b, Pik3cb, Csf2ra, Fuca1, Dusp3, Rab31, Dock5, Themis2, Adam8, Itgam, Irf5, Ceacam1, Ccnd1, Tbc1d8, Card9, Laptm4b, Pak1, Mx1, Il12rb1, Inppl1, Rgs1, Ifng, Itgax, Fgr, Pmaip1, Slc7a7, Cd68, Tlr4, Galnt3, Plxnb2, Cd300a, Fcer1g, Dusp4, Rgs16, Ptger2, E2f3, Myb, Nr4a2, Cdc25b, Casp3, Spock2, Ezh2, Kif22, Il2ra, Cd40lg, Csf1, Hemgn, Rora, Casp1, Cx3cr1, Gzmb, Mdfic, Ptpn3, Ahr, Litaf, Ctnna1, Vegfa, Dusp9, Gale, Irf4, S100a4, Pask, Clspn, E2f2, Psat1, Cenpi, Cdk1, Ttk, S100a11, Evi2a, Pkig, Bhlhe40, Ccl3

Table 3. Upregulated DEGs in naive vs TM CD8 T cells

	Name	P-value	Adjusted P-value	Odds Ratio	Combined Score	Genes
1	Cyanoamino acid metabolism	0.004222	0.858312	27.27197	149.1096	GGT5;GGT1
2	Taurine and hypotaurine metabolism	0.00879	0.858312	17.04239	80.682	GGT5;GGT1
3	Glutathione biosynthesis and recycling	0.01064	0.858312	15.14802	68.81916	GGT5;GGT1
4	Osteoblast signaling	0.017107	0.999958	11.35928	46.21276	PDGFRB;COL1A1
5	Beta-3 integrin cell surface interactions	0.024518	0.999958	5.122135	18.99471	PDGFRB;COL1A1;PLAUR
6	Glutathione conjugation	0.05081	0.999958	5.923274	17.64936	GGT5;GGT1
7	Arachidonic acid metabolism	0.052381	0.999958	3.722348	10.97803	GGT5;PLA2G4B;GGT1
8	Selenoamino acid metabolism	0.054529	0.999958	5.676182	16.51219	GGT5;GGT1
9	G2 phase pathway	0.07067	0.999958	16.98707	45.01118	CCNA1
10	Histidine catabolism	0.07067	0.999958	16.98707	45.01118	HAL

IL-15 is essential for the development and/or survival of Ly6C$^+$ VM CD8 cells

To compare the characteristics of Ly6C$^+$ (Q1 and Q2) and Ly6C$^-$ (Q3 and Q4) subsets of VM CD8 T cells, 481 and 1,002 upregulated genes in Ly6C$^+$ and Ly6C$^-$ subsets, respectively, were collected and pathway analysis was performed using Bioplanet 2019. The top 10 signaling pathways, which were upregulated in each subset are shown in Figure 11 and Tables 4 and 5. Consistent with the findings in Figure 10A, all of the top 10 pathways upregulated in the Ly6C$^-$ subsets were related to the cell cycle (Figure 11, Table 4). In contrast, only a limited number of genes were found to be upregulated in the top 10 pathways in Ly6C$^+$ VM cells (Table 5). To further explore the role of IL-15, IL-15 related genes were compiled from previous studies (Table 6) and their expression was compared among CD8 T cell subsets (Figure 12A). IL-15 receptor consists of the unique IL-15Rα subunit (encoded by the *Il15ra* gene) and the shared receptor complex including IL-2/IL-15Rβ (CD122 encoded by the *Il2rb* gene) and IL2Rγ (common γ chain encoded by the *Il2rg* gene), which are also shared by the IL-2. The heatmap analysis revealed higher levels of *Il2rb, Il15ra,* and *Il7r* (encoding IL-7Rα, CD127) genes compared with other subsets in Ly6C$^+$ VM CD8 T cells (Q1 and Q2), while *Il2ra* and *bcl6* gene expression was upregulated in both Ly6C$^-$ (Q3 and Q4) VM and TM cells, suggesting that Ly6C$^+$ VM CD8 T cells may

rely more on IL-15 signaling than other subsets for their development and maintenance. In addition, the expression of *Bcl2, Runx2* and *Eomes* genes was also higher in Ly6C$^+$ VM CD8 T cells than in other subsets. The anti-apoptotic *Bcl2* gene has been reported to be upregulated by IL-15 via an mTOR-independent pathway [53-55]. *Runx2,* which is also induced by IL-15, is important for maintenance of long-term memory CD8 T cells [56, 57]. *Eomes* and *Il2rb* gene expression is essential for the CD8 T cell response to IL-15 [13, 58]. Flow cytometric analysis further confirmed the higher expression of these proteins in Ly6C$^+$ (Q1 and Q2) VM cells than in other CD8 T cell subsets (Figure 12B). The expression of *Eomes* genes in CD8 T cells is associated with effector function [59]. Ly6C expression in memory CD8 T cells has been reported to correlate with increased IFN-γ production [60]. Accordingly, upon stimulation with PMA and ionomycin, Ly6C$^+$ VM CD8 T cells (Q1 and Q2) expressed higher levels of IFN-γ, TNF-α, and perforin than in Ly6C$^-$ VM cells (Q3 and Q4) (Figure 12C). In contrast, the production of IFN-γ in Ly6C$^-$ VM CD8 T cells was very low, similar to that of naïve CD8 T cells. These results suggest that Ly6C$^+$ VM T cells exhibit rapid and immediate response to foreign antigens or upon cytokine stimulation. Considering that cytokines such as IL-15 and IL-18 activate memory-like CD8 T cells even in the absence of TCR stimulation [44], the upregulated expression of *Il2rb* (Figure 12A) and *Il18r1* (Table 5) genes

in Ly6C$^+$ VM T cells further supports the role of these cells as bystander-activated cells.

In addition to the well-known IL-15-related genes, the *Mst1* gene is of particular interest. Mst1 is a member of the Hippo pathway, which responds to various intracellular and extracellular signals through Yap/Taz (Yes-associated protein 1/WW domain-containing transcription regulator 1) [61]. Interestingly, it has been reported that Mst1 induces cellular quiescence by suppressing proliferation and supporting cell survival via the upregulation of Bcl-2 expression in response to IL-15 during the development of type I invariant NKT cells [62]. The same study also demonstrated that Mst1 enhances IL-15-STAT5 signaling, leading to the upregulation of *Il2rb* gene. These findings suggest that Mst1-mediated IL-15 signaling may upregulate *Il2rb* and *bcl2* gene expression in Ly6C$^+$ VM cells, promoting cell survival while suppressing the expression of cell cycle-related genes, thereby inducing cellular quiescence. To investigate this further, CD8 T cell subsets were stimulated with IL-15, and the phosphorylation of Mob1, a target of Mst1, was assessed by flow cytometry. As expected, Ly6C$^+$ VM cells exhibited higher levels of Mob1 protein phosphorylation compared with the other CD8 T cell subsets, while no significant difference was found between Ly6C$^-$ VM cells and naïve cells (Figure 13A). WT CD8 T cell subsets were then isolated and cultured in the presence of IL-15 for 3 days,

followed by assessment of cell survival using Annexin V and 7-AAD staining. In the absence of IL-15 in the culture media, Ly6C$^+$ cells showed the highest levels of apoptosis across all subsets, whereas the addition of IL-15 most effectively rescued the viability of the Ly6C$^+$ subset (Figure 13B). Taken together, these findings suggest that Ly6C$^+$ VM CD8 T cells are strongly dependent on IL-15 signaling for their development, survival, and function than other CD8 T cell subsets.

Next, RNA sequencing data from Ly6C$^+$ VM CD8 T cells were further analyzed to compare the characteristics of IL-4-dependent (Q1, Ly6C$^+$ Sca-1$^-$) and type I IFN-dependent (Q2, Ly6C$^+$ Sca-1$^+$) VM CD8 T cells. A total of 394 DEGs were identified. Analysis using Bioplanet 2019 revealed the top 10 signaling pathways, which were upregulated in Ly6C$^+$ Sca-1$^-$ (Q1) and Ly6C$^+$ Sca$^-$1$^+$ (Q2) cells (Figure 14). The pathways upregulated in Ly6C$^+$ Sca-1$^-$ (Q1) did not exhibit a significant number of DEGs (Table 7). However, the *innate immune system* and the *adoptive immune system* pathways, which included genes such as *Cd80* and *Cd81*, were identified as the major upregulated pathways in the Ly6C$^+$ Sca-1$^+$ (Q2) subset (Table 8). CD80 and CD81 proteins are T cell costimulatory molecules that play a role in T cell activation via distinct pathways. CD81 costimulation has been reported to increase IFN-γ and TNF-α production without significantly affecting IL-2 production [63, 64].

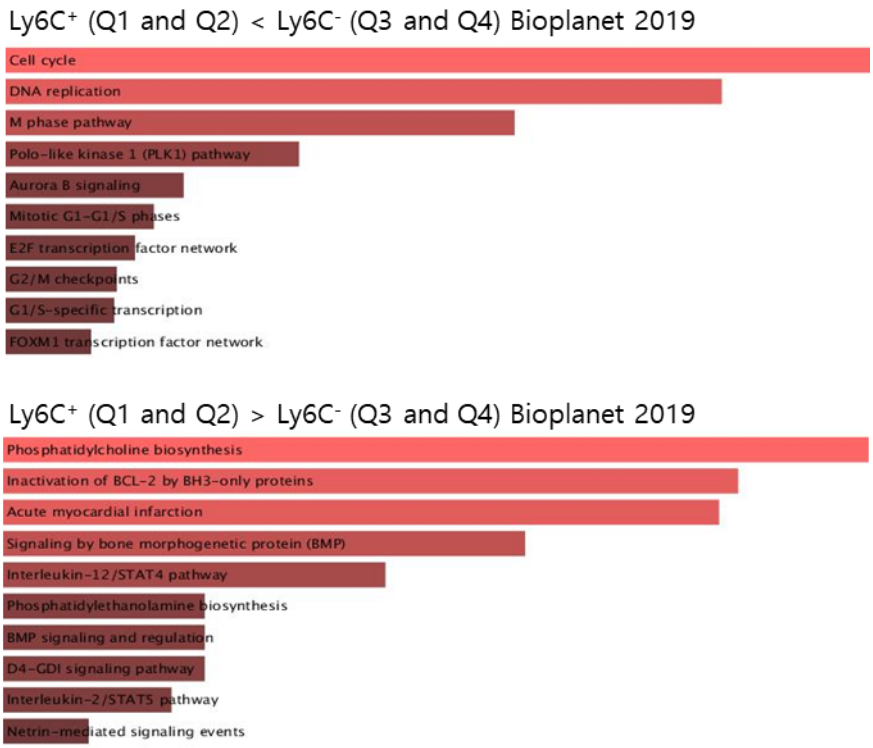

Figure 11. Pathway analysis highlighted the top 10 enriched pathways in Ly6C$^+$ and Ly6C$^-$ VM cells. Enrichr bar graph, generated using Bioplanet 2019, displays the pathways that were upregulated in Ly6C$^-$ (Q3 and Q4) VM cells (upper) and Ly6C$^+$ (Q1 and Q2) VM cells (lower) of WT B6 mice. The length of the bars represents the significance of each pathway, with longer bars indicating greater significance

Table 4. Upregulated DEGs in Ly6C$^-$ (Q3 and Q4) vs Ly6C$^+$ (Q1 and Q2) VM CD8 T cells

	Name	P-value	Adjusted P-value	Odds Ratio	Combined Score	Genes
1	Cell cycle	4.68E-30	4.73E-27	5.066061	342.1364	TOP2A;CDKN1A;FEN1;ERCC6L;MCM7;ZWILCH;GMNN;BUB1B;MCM10;BRCA1;CKS1B;LMNB1;CDC20;CCND1;MIS18BP1;NUF2;CHEK1;NEK2;OIP5;KNTC1;MYBL2;SPDL1;FBXO5;POLE;RFC3;LIG1;H2AFX;TBC1D8;KIF23;CCNA2;ESPL1;CCNE2;INCENP;GORASP1;MCM3;BIRC5;MCM5;KIF2C;DNA2;KIF20A;PRIM1;CDCA8;TTK;TYMS;CENPA;SKA1;NSL1;AURKB;AURKA;CCNB2;SYCE2;CCNB1;CDC45;ORC1;PRKAR2B;LMNA;E2F1;E2F2;CLSPN;BUB1;GINS1;GINS2;CDKN2C;RRM2;GADD45B;TGFB3;UBE2C;PLK1;CDC6;HSPA2;TUBB4A;NDC80;DHFR;CENPE;POLA1;CENPF;KIF18A;WEE1;CENPH;CENPI;ALMS1;CENPK;CDK2;CDK1;CENPM;CENPN;CENPP;SPC24;MAD2L1;SPC25
2	DNA replication	4.81E-26	2.44E-23	7.3886	430.723	CDKN1A;FEN1;ERCC6L;MCM7;ZWILCH;GMNN;BUB1B;MCM10;CDC20;NUF2;KNTC1;FBXO5;SPDL1;POLE;RFC3;LIG1;KIF23;CCNA2;INCENP;GORASP1;MCM3;BIRC5;KIF2C;MCM5;DNA2;KIF20A;PRIM1;CDCA8;CENPA;SKA1;AURKB;NSL1;CDC45;ORC1;E2F1;E2F2;BUB1;GINS1;GINS2;PLK1;CD

						C6;NDC80;POLA1;CENPE;CENPF;KIF18A;CENPH;CENPI;CENPK;CDK2;CENPM;CENPN;CENPP;SPC24;MAD2L1;SPC25
3	M phase pathway	1.95E-20	6.57E-18	10.72754	486.8726	ERCC6L;ZWILCH;BUB1B;CDCA8;CENPA;AURKB;NSL1;SKA1;CDC20;NUF2;KNTC1;FBXO5;SPDL1;BUB1;PLK1;KIF23;NDC80;CENPE;CENPF;KIF18A;CENPH;INCENP;CENPI;GORASP1;CENPK;BIRC5;CENPM;KIF2C;CENPN;KIF20A;CENPP;SPC24;MAD2L1;SPC25
4	Polo-like kinase 1 (PLK1) pathway	1.34E-14	3.38E-12	14.86135	474.7701	ERCC6L;PLK1;BUB1B;NDC80;AURKA;CDC20;CENPE;TPX2;CCNB1;WEE1;INCENP;PRC1;GORASP1;CDK1;CLSPN;FBXO5;KIF20A;ECT2;BUB1;SPC24
5	Aurora B signaling	1.78E-11	3.60E-09	13.38742	331.3826	CDCA8;NCAPG;KIF23;CENPA;AURKB;NCAPH;NDC80;AURKA;SMC2;INCENP;STMN1;BIRC5;KIF2C;NCAPD2;KIF20A;BUB1
6	Mitotic G1-G1/S phases	1.14E-10	1.92E-08	5.0754	116.2093	TOP2A;CDKN1A;MCM7;PRIM1;MCM10;TYMS;CKS1B;CCNB1;CDC45;CCND1;ORC1;E2F1;E2F2;MYBL2;FBXO5;POLE;CDKN2C;RRM2;CDC6;DHFR;CCNA2;POLA1;WEE1;CCNE2;CDK2;CDK1;MCM3;MCM5
7	E2F transcription	3.68E-10	5.32E-08	7.144905	155.2067	CDKN1A;RRM1;CDKN2C;RRM2;BRCA1;CDC6;TYMS;HIC1;CCNA2;POLA1;CCNE2;ORC1;CDK2;MCM3;E2F1;CDK1;E2F2;MYBL2;TK1;E2F7

	factor network					
8	G2/M checkpoints	1.15E-09	1.45E-07	10.29635	211.9688	RFC3;MCM7;MCM10;CDC6;CCNB2;CCNB1;WEE1;CDC45;ORC1;CHEK1;CDK2;CDK1;MCM3;MCM5;CLSPN
9	G1/S-specific transcription	1.34E-09	1.51E-07	27.34879	558.6712	DHFR;POLA1;RRM2;CDC45;ORC1;CDK1;E2F1;CDC6;FBXO5;TYMS
10	FOXM1 transcription factor network	5.68E-09	5.75E-07	9.95629	189.0306	PLK1;FOXM1;CENPA;AURKB;CKS1B;CCNA2;CCNB2;CCNB1;CENPF;CCND1;CDK2;CDK1;BIRC5;NEK2

Table 5. Upregulated DEGs in Ly6C$^+$ (Q1 and Q2) vs Ly6C$^-$ (Q3 and Q4) VM CD8 T cells

	Name	P-value	Adjusted P-value	Odds Ratio	Combined Score	Genes
1	Phosphatidylcholine biosynthesis	0.00862	0.999996	8.160669	38.79267	CHPT1;LPIN1;LPIN3
2	Inactivation of BCL-2 by BH3-only proteins	0.011188	0.999996	16.29562	73.21492	BCL2;BBC3
3	Acute myocardial infarction	0.011623	0.999996	7.199852	32.07344	PROS1;F2R;PLAT
4	Signaling by bone morphogenetic protein (BMP)	0.017124	0.999996	6.118933	24.88745	FSTL1;ACVR2A;BMPR1A
5	Interleukin-12/STAT4 pathway	0.022641	0.999996	3.983842	15.09083	IL18RAP;TBX21;PRF1;IL18R1
6	Phosphatidylethanolamine biosynthesis	0.03248	0.999996	8.14572	27.91643	LPIN1;LPIN3
7	BMP signaling and regulation	0.03248	0.999996	8.14572	27.91643	RUNX2;BMPR1A
8	D4-GDI signaling pathway	0.03248	0.999996	8.14572	27.91643	PRF1;ARHGAP5
9	Interleukin-2/STAT5 pathway	0.034713	0.999996	4.530916	15.22683	IL2RB;PRF1;BCL2
10	Netrin-mediated signaling events	0.040952	0.999996	4.218006	13.47804	YES1;CAMK2A;PTK2

Table 6. IL-15-related genes compiled from literature

	Genes	Ref
IL-2/IL-15 receptor related gene	Il15ra, Il2rg, Il2ra, Il2rb, Eomes, Bcl2, runx2, Bcl6	T. Hussain et al., 2019; E. Olesin et al., 2018; W. Zhao et al., 2021; I. D. Cooley et al., 2015
VM related genes	Ccl3, Ccl4, Ccl5, Ccr5, Cd27, Cxcr3, Cxcr5, Eomes, Fasl, Gzmb, Ifnar2, Ifng, Ifngr1, Il10ra, Il10rb, Il12rb1, Il18r1, Il18rap, Il2rb, Il3ra, Il4ra, Il7r, NKG2D, Pdgfb, Stat1, Stat2, Stat3 Stat4, Stat5a, Stat5b, Tbx21,Tnf, Tnfrsf1b, Tnfrsf25, Tnfrsf9, Tnfsf10, Tnfsf14, Tnfsf8, Xcl1	J. T. White et al., 2016
Hippo pathway gene in IL-15 signaling	mst1	L. Van Kaer et al., 2020

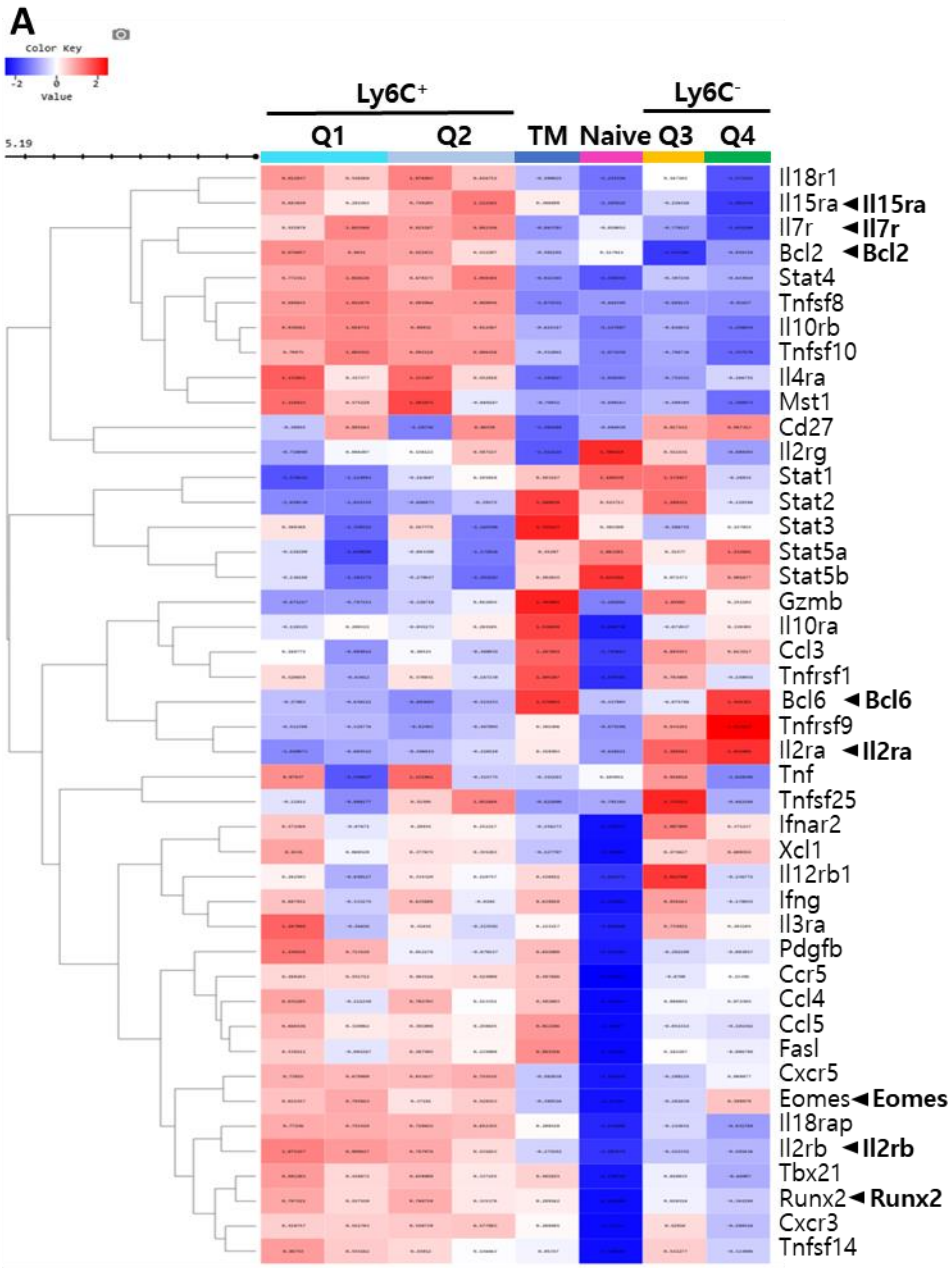
A
Color Key
-2
0
2
value
5.19
Ly6C+
Ly6C-
Q1
Q2
TM
Naive
Q3
Q4
Il18r1
Il15ra
Il15ra
Il7r
Il7r
Bcl2
Bcl2
Stat4
Tnfsf8
Il10rb
Tnfsf10
Il4ra
Mst1
Cd27
Il2rg
Stat1
Stat2
Stat3
Stat5a
Stat5b
Gzmb
Il10ra
Ccl3
Tnfrsf1
Bcl6
Bcl6
Tnfrsf9
Il2ra
Il2ra
Tnf
Tnfsf25
Ifnar2
Xcl1
Il12rb1
Ifng
Il3ra
Pdgfb
Ccr5
Ccl4
Ccl5
Fasl
Cxcr5
Eomes
Eomes
Il18rap
Il2rb
Il2rb
Tbx21
Runx2
Runx2
Cxcr3
Tnfsf14

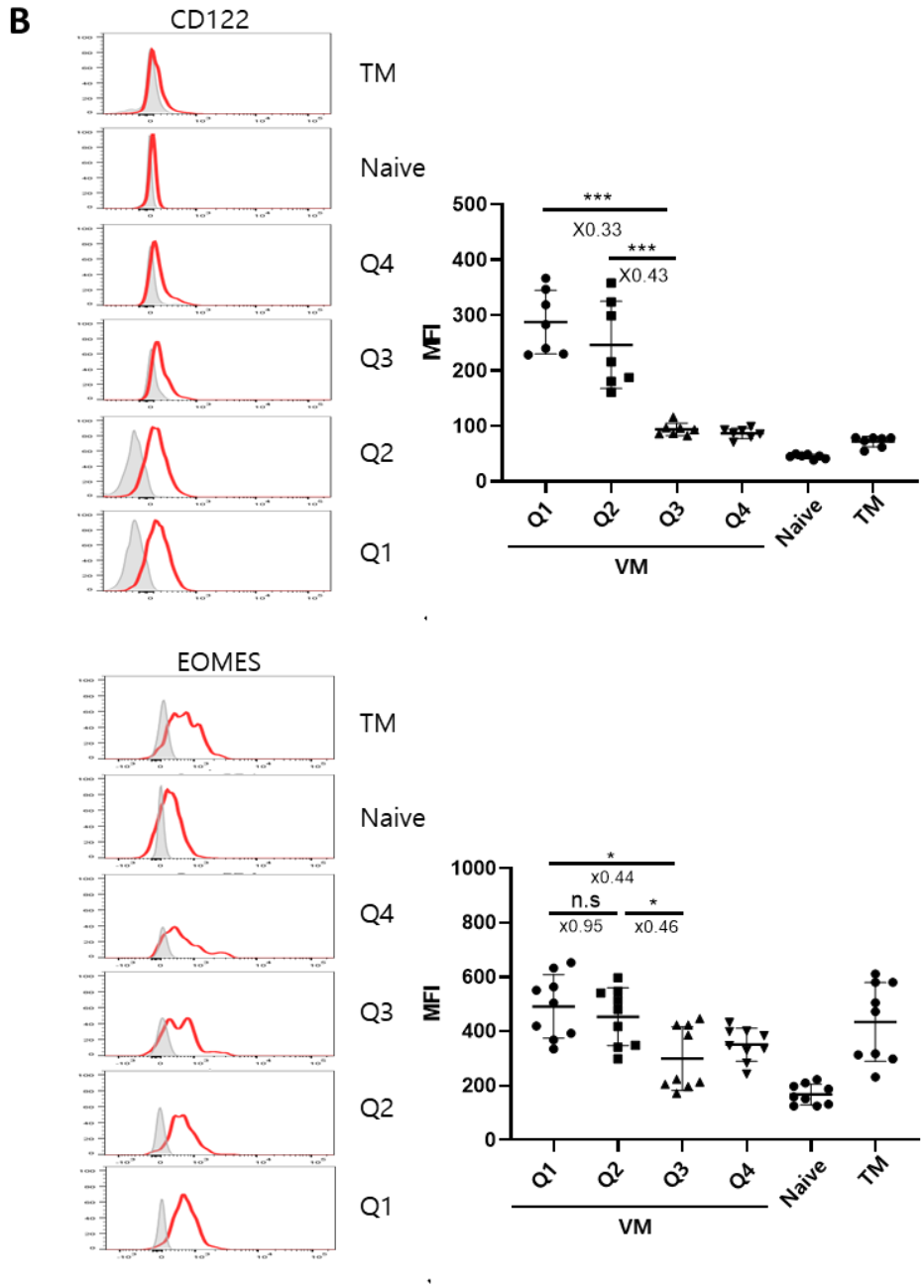
B
CD122
TM
Naive
Q4
Q3
Q2
Q1
MFI
500
400
300
200
100
0
***
X0.33
***
X0.43
Q1
Q2
Q3
Q4
Naive
TM
VM
EOMES
TM
Naive
Q4
Q3
Q2
Q1
MFI
1000
800
600
400
200
0
*
x0.44
n.s
x0.95
*
x0.46
Q1
Q2
Q3
Q4
Naive
TM
VM

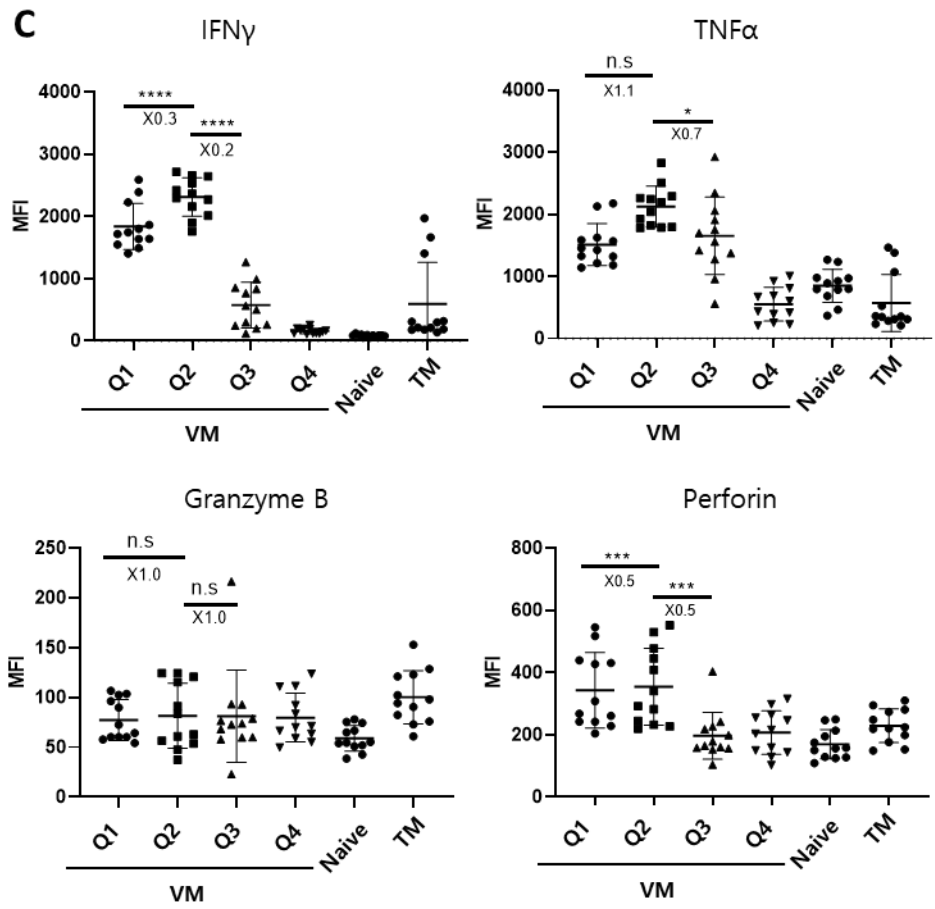

Figure 12. IL-15 plays an essential role in the development Ly6C^{+} VM CD8 cells. (A) The heatmap shows the differential expression of 44 IL-15-related genes listed in Table 10 between different CD8 T cell subsets. (B) Flow cytometric analysis was performed to compare the expression levels of CD122 and EOMES in CD8 T cell subsets of WT B6 mice. The representative histogram and a summarized graph of median fluorescence intensity (MFI) are shown. The grey lines represent the negative control, and all MFIs are calculated by subtracting the MFI

of the negative control. (C) Splenocytes were stimulated with a PMA/ionomycin cocktail for 5 hours in the presence of Golgiplug. The cells were then stained with antibodies against IFN-γ, TNF-α, granzyme B, and perforin. The median fluorescence intensity (MFI) of each cytokine expression is shown in a summarized graph. Summarized data (n= 12/group) are presented as mean ± SD with the fold changes between the two groups indicated by the x-numbers. Statistical analyses were measured using an unpaired t-test and Mann-Whitney test. n.s, not significant. *$p < 0.05$; ***$p < 0.001$; ****$p < 0.0001$.

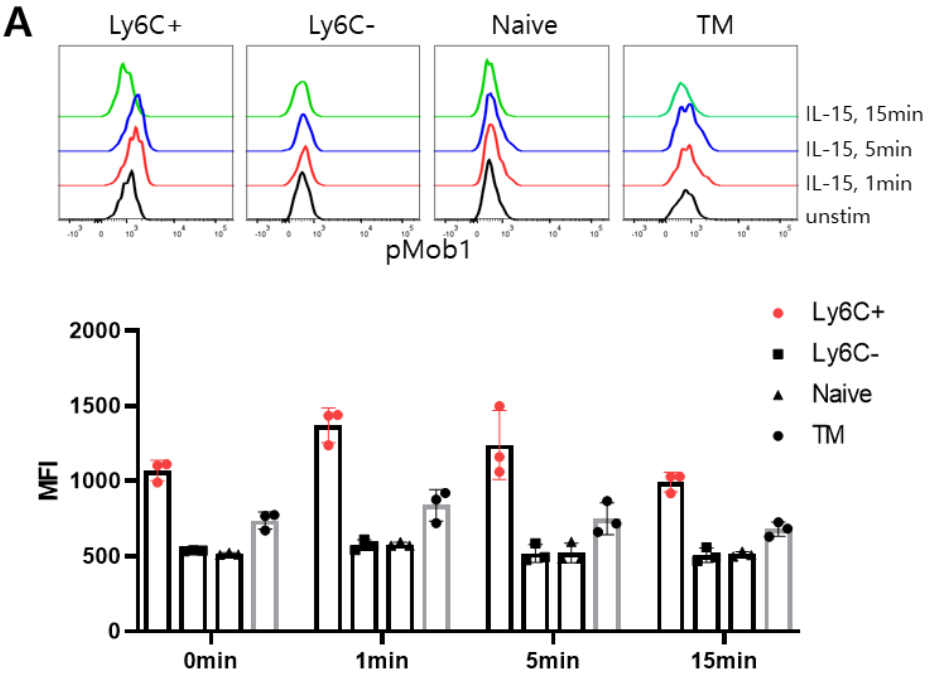
A
Ly6C+
Ly6C-
Naive
TM
IL-15, 15min
IL-15, 5min
IL-15, 1min
unstim
pMob1
Ly6C+
Ly6C-
Naive
TM
MFI
2000
1500
1000
500
0
0min
1min
5min
15min

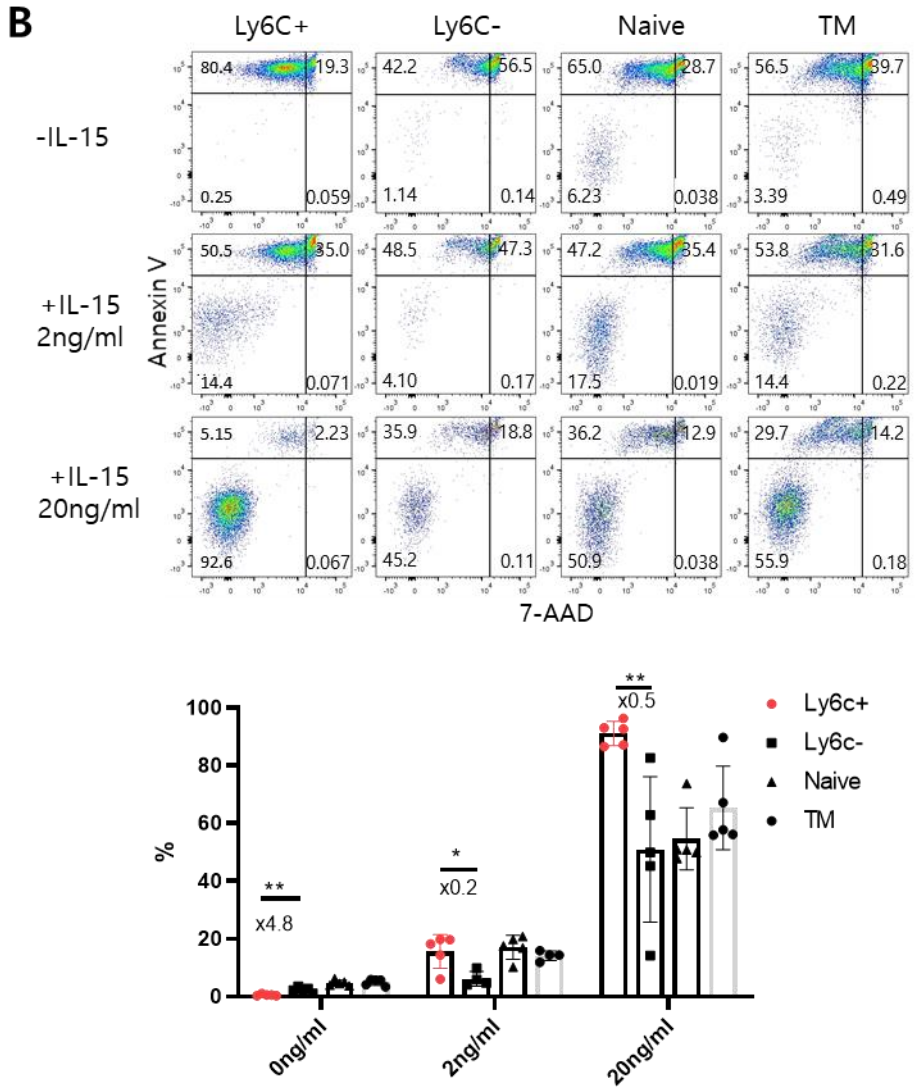

Figure 13. Survival of Ly6C$^+$ VM CD8 cells is IL-15 dependent. (A) Total splenocytes were cultured with IL-15 for the indicated time and then stained with an anti-phosphorylated Mob1 (pMob1) antibody. The expression levels of pMob1 in the different CD8 T cell subsets were analyzed by flow cytometry. Representative histograms and a summarized graph of the median fluorescence intensity (MFI) are shown.

(B) Splenic CD8 T cells were sorted into naïve, TM, Ly6C^{+} VM and Ly6C^{-} VM cells by FACS sorter and cultured with or without 2 ng or 20ng/ml of hIL-15 for 3 days. The viability of each subsets was assessed by 7-AAD and Annexin V. Representative plots and summarized data are shown. The numbers within the plots indicate the percentage of cells within each quadrant. Summarized data (n=3-4/group) are presented as mean ± SD with the fold changes between the two groups indicated by the x-numbers. Statistical analyses were performed using an unpaired t-test and Mann-Whitney test. *$p < 0.05$; **$p < 0.01$.

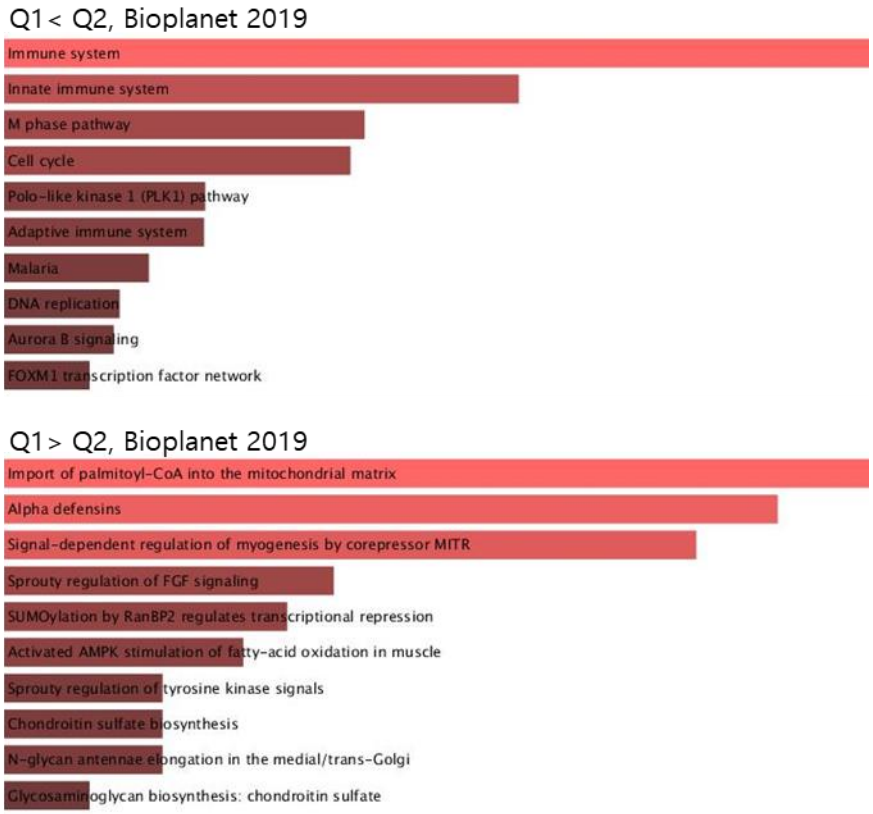

Figure 14. Pathway analysis of RNA-Seq results presented the enriched pathway between IL-4-dependent (Ly6C$^+$ Sca-1$^-$) and type I IFN-dependent (Ly6C$^+$ Sca-1$^+$) VM CD8 T cell subsets. The analysis was conducted using the Bioplanet 2019 tool, and the top 10 pathways that were upregulated in the Ly6C$^+$ Sca-1$^+$ subset (Q2, upper) and in the Ly6C$^+$ Sca-1$^-$ subset (Q1, lower) are presented. The length of the bars represents the significance of each pathway, with longer bars indicating greater significance.

Table 7. Upregulated DEGs in Ly6C^{+} Sca-1^{-} (Q1) vs Ly6C^{+} Sca-1^{+} (Q2) VM CD8 T cell subsets

	Name	P-value	Adjusted P-value	Odds Ratio	Combined Score	Genes
1	Import of palmitoyl-CoA into the mitochondrial matrix	0.016286	0.289896	71.25714	293.3998	CPT1B
2	Alpha defensins	0.018303	0.289896	62.34688	249.4308	ART1
3	Signal-dependent regulation of myogenesis by corepressor MITR	0.020316	0.289896	55.41667	215.9217	HDAC9
4	Sprouty regulation of FGF signaling	0.032312	0.289896	33.24	114.09	SPRY2
5	SUMOylation by RanBP2 regulates transcriptional repression	0.034298	0.289896	31.16094	105.0959	HDAC9
6	Activated AMPK stimulation of fatty-acid oxidation in muscle	0.036279	0.289896	29.32647	97.26176	CPT1B
7	Sprouty regulation of tyrosine kinase signals	0.04023	0.289896	26.23684	84.30285	SPRY2
8	Chondroitin sulfate biosynthesis	0.04023	0.289896	26.23684	84.30285	CHST3
9	N-glycan antennae elongation in the medial/trans-Golgi	0.04023	0.289896	26.23684	84.30285	ST8SIA6
10	Glycosaminoglycan biosynthesis: chondroitin sulfate	0.044165	0.289896	23.73571	74.05131	CHST3

Table 8. Upregulated DEG in Ly6C^{+} Sca-1^{+} (Q2) vs Ly6C^{+} Sca-1^{-} (Q1) VM CD8 T cell subsets

	Name	P-value	Adjusted P-value	Odds Ratio	Combined Score	Genes
1	Immune system	8.40E-11	6.12E-08	3.175788	73.67857	CD81;NCF2;CD80;UBE2L6;KIF11;KIF15;LGALS3;MRC1;IGLC3;CASP1;CTSH;IGLC1;IGLC2;TICAM2;SYK;IFNGR2;CD180;CYBB;IRAK3;GAB2;HCK;RNF144B;TYROBP;IL1B;BTK;TLR9;KIF2C;IRF5;KIF20A;TLR4;C1QB;C1QA;SRC;CSF2RB;C2;C3;IGKC;CD14;LYN;CD74;VCAM1;UBE2C;LY86;CD4;CD40LG;CDK1;ASB2;LGMN;C1QC
2	Innate immune system	1.34E-08	4.90E-06	4.556439	82.58847	C1QB;C1QA;TICAM2;CD180;LY86;UBE2L6;IRAK3;C2;C3;LGALS3;CD4;IGKC;BTK;TLR9;CDK1;CASP1;IGLC3;IGLC1;CD14;IGLC2;TLR4;LGMN;C1QC
3	M phase pathway	1.25E-07	2.80E-05	8.195643	130.2463	CENPF;GORASP1;NUF2;BIRC5;CDCA8;CENPM;KNTC1;KIF2C;KIF20A;BUB1;AURKB;SPC24
4	Cell cycle	1.54E-07	2.80E-05	3.578913	56.14222	TOP2A;CDCA8;MCM10;TTK;AURKB;CCND1;ORC1;NUF2;KNTC1;NEK2;CLSPN;BUB1;RRM2;UBE2C;TBC1D8;MPEG1;CCNA2;CENPF;ESPL1;GORASP1;CDK1;CENPM;BIRC5;KIF2C;KIF20A;SPC24

5	Polo-like kinase 1 (PLK1) pathway	1.26E-06	1.56E-04	11.96583	162.5039	TPX2;PRC1;GORASP1;CDK1;CLSPN;KIF20A;BUB1;SPC24
6	Adaptive immune system	1.29E-06	1.56E-04	2.958202	40.12531	CD81;NCF2;SRC;CD80;UBE2L6;KIF11;KIF15;C3;IGKC;MRC1;IGLC3;CTSH;IGLC1;IGLC2;LYN;CD74;VCAM1;SYK;UBE2C;CYBB;RNF144B;CD4;CD40LG;TYROBP;BTK;KIF2C;KIF20A;ASB2;LGMN
7	Malaria	2.86E-06	2.98E-04	10.57176	134.9518	VCAM1;CD40LG;LRP1;CD81;IL1B;SDC3;TLR9;TLR4
8	DNA replication	4.37E-06	3.85E-04	4.49681	55.49587	CDCA8;MCM10;AURKB;CCNA2;CENPF;ORC1;GORASP1;NUF2;CENPM;BIRC5;KIF2C;KNTC1;KIF20A;BUB1;SPC24
9	Aurora B signaling	4.76E-06	3.85E-04	12.4011	151.9889	CDCA8;NCAPG;BIRC5;KIF2C;KIF20A;BUB1;AURKB
10	FOXM1 transcription factor network	6.74E-06	4.92E-04	11.67044	138.9575	CCNA2;CENPF;CCND1;CDK1;BIRC5;NEK2;AURKB

Ly6C$^-$ VM cells, in contrast to the Ly6C$^+$ subset, are sensitive to exogenous IL-4.

The development of Ly6C$^+$ Sca-1$^-$ (Q1) and Ly6C$^+$ Sca-1$^+$ (Q2) VM CD8 cells depends on cytokine expression. Therefore, the expression patterns of IL-4 and type I IFN receptors were investigated. Unexpectedly, both the receptor gene (*Il4ra*) and the corresponding protein (CD124) for IL-4 were found to be highly expressed in both subsets compared with the other subsets (Figure 15 A and B, left). However, no significant differences were found in the expression of IFNAR1, the receptor for both IFN-α and IFN-β, between the different VM cell subsets (Figure 15B, right).

In an earlier experiment using an influenza infection model, administration of IL-4C in vivo led to a significant increase in CXCR3 expression in both naive and memory phenotype wells, thereby facilitating their migration to inflamed lungs (Figure 3 A and B). The pattern of IL-4Rα (CD124) expression suggested that exposure to exogenous IL-4 could expand Ly6C$^+$ VM cells. To investigate this possibility, the expression of CXCR3 was compared between naive and IL-4C treated mice. Consistent with the gene expression pattern (Figure 10), CXCR3 expression was the highest in the Ly6C$^+$ (Q1 and Q2) VM CD8 T cell subsets of naive mice, followed by the Ly6C$^-$ Sca-1$^+$ (Q3) subset, while it was very low in the Ly6C$^-$ Sca-1$^-$ (Q4) subset (Figure

16A). However, administration of IL-4C increased the expression of CXCR3 in the $Ly6C^-$ VM (Q3 and Q4) subsets and naive cells, resulting in levels similar to those observed in $Ly6C^+$ VM (Q1 and Q2) cells. Further, IL-4C treatment increased the total number of splenocytes, CD8 T cells, and VM cells (Figure 16B); it primarily expanded the $Ly6C^-$ VM (Q3 and Q4) population, while the $Ly6C^+$ VM (Q1 and Q2) population remained largely unaffected (Figure 16C and D). These results contradict the effects of endogenous IL-4 observed in IL-4 KO mice. IL-4Rα expression is known to be upregulated by IL-4 itself [65, 66]. As shown in Figure 15B, the $Ly6C^+$ subsets express higher levels of IL-4Rα expression compared with the $Ly6C^-$ subsets, suggesting prior exposure of the $Ly6C^+$ subsets to higher IL-4 signal in vivo. Therefore, it is possible that they do not respond to exogenous IL-4 due to saturation of IL-4Rα signaling.

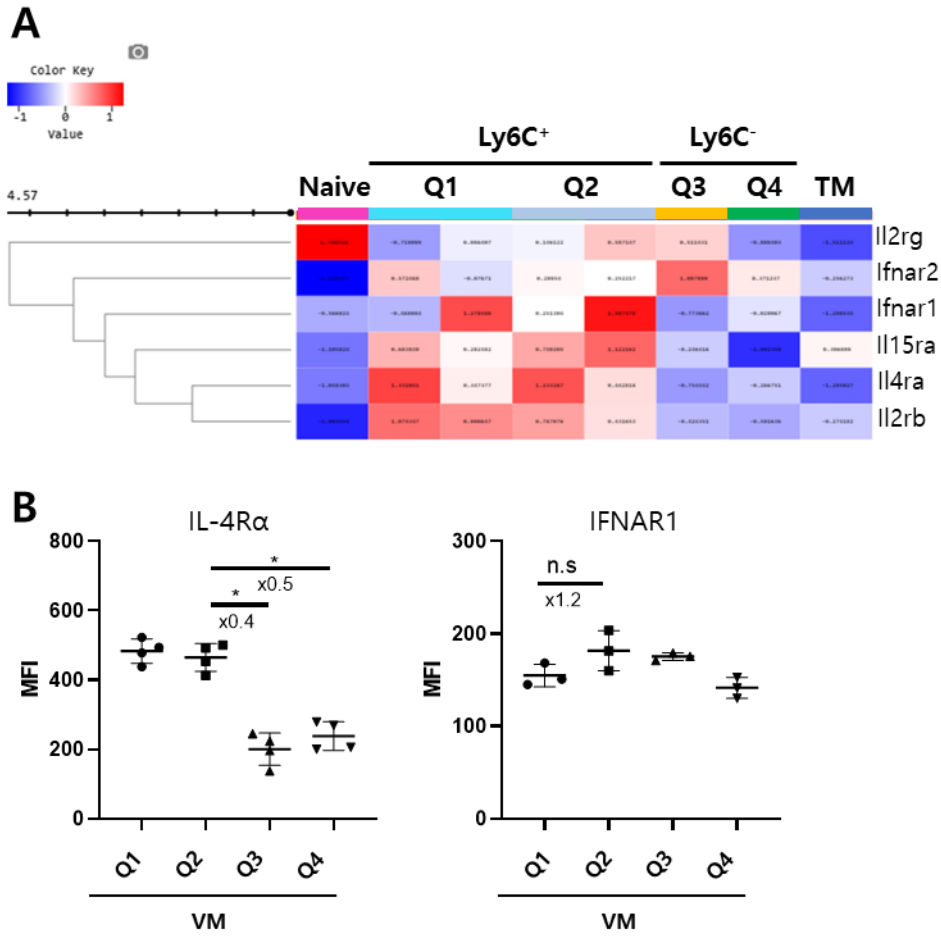

Figure 15. IL-4R, but not type 1 IFN receptor, is differentially expressed in VM CD8 T cell subsets. (A) The expression profile of cytokine receptors genes for IL-4, type I IFN and IL-15 are present as a heatmap. (B) Flow cytometric analysis was performed to compare the expression levels of CD124 (IL-4Rα, encoded by the Il4ra gene) (left) and IFNAR1 (receptor for both IFN-α and IFN-β, encoded by the Ifnar1 gene) (right) proteins in each subset of CD8 T cells. The median fluorescence intensity (MFI) was calculated by subtracting the MFI of

the negative control, and the summarized graphs show the MFI for each subset. The summarized data (n=3-4/group) are presented as mean ± SD and the fold changes between the two groups are indicated by the x-numbers. Statistical analyses were measured using an unpaired t-test and Mann-Whitney test. n.s, not significant. *$p < 0.05$.

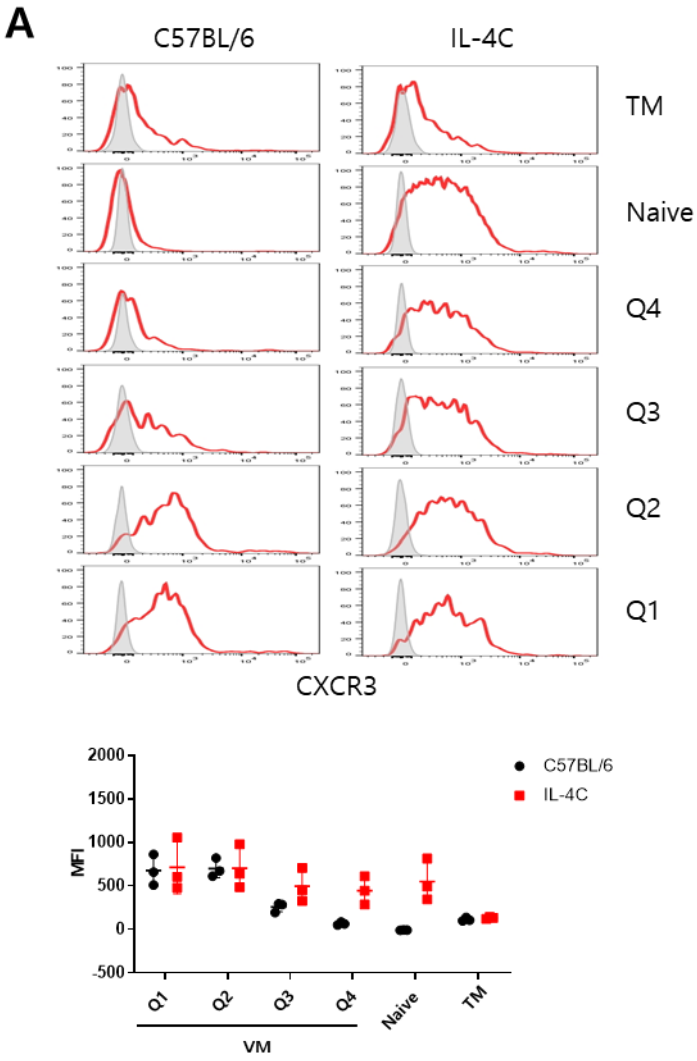
A
C57BL/6
IL-4C
TM
Naive
Q4
Q3
Q2
Q1
CXCR3
2000
1500
1000
500
0
-500
MFI
C57BL/6
IL-4C
Q1
Q2
Q3
Q4
Naive
TM
VM

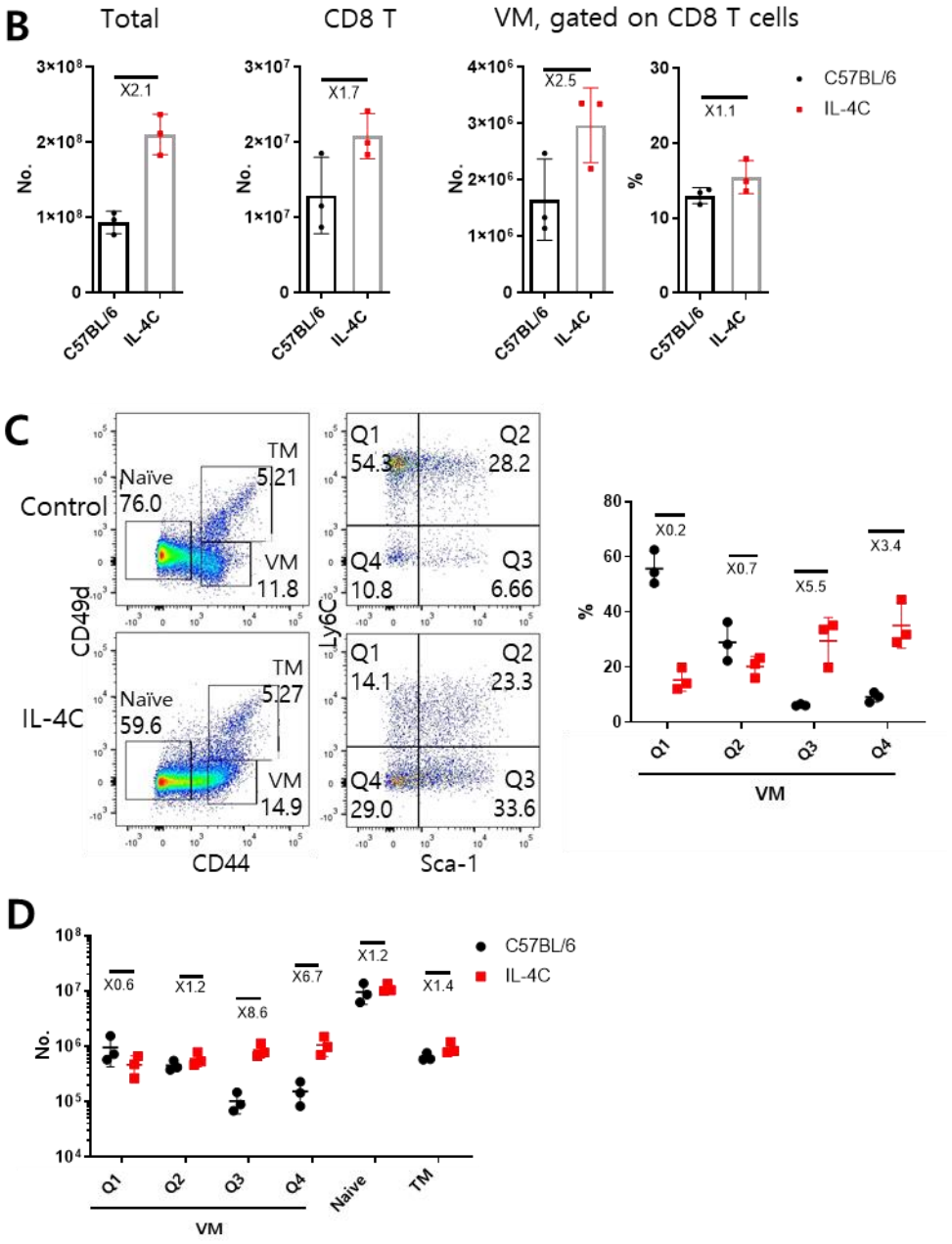

Figure 16. Exogenous IL-4 treatment primary affects Ly6C$^-$ VM CD8 T cells. IL-4C was administered to C57BL/6 mice for 7 days, similar to the experimental setup shown in Figure 1A. Flow cytometric

analysis was performed to compare CXCR3 expression and changes in the VM cell population between naive and IL-4C-treated mice. (A) The representative histogram and summarized graph show the expression of CXCR3, represented by the median fluorescence intensity (MFI). (B) The summarized graph illustrates the total number of splenocytes, CD8 T cells, and VM CD8 T cells, as well as the percentage of VM CD8 T cells. (C) Representative dot plots illustrate the frequency of the different subsets of CD8 T cells, including naive, VM and TM populations (left) and the subsets within VM cells (right). The frequency of VM subsets is presented as a graph. (D) The summarized graph displays the absolute number of each CD8 T cell subset. The numbers within the plots indicate the percentage of cells within each rectangle or quadrant. Summarized data (n=3/group) are presented as mean ± SD with the fold changes between the two groups indicated by the x-numbers. Statistical analyses were performed using an unpaired t-test and Mann-Whitney test. n.s, not significant. *$p < 0.05$. **$p < 0.001$.

Complement pathway is predominant in Sca-1$^+$ VM CD8 T cells.

In the absence of type I IFN signal, significant decrease was observed in the number of Sca-1$^+$ VM CD8 T cells (Figure 6). RNA sequencing data were analyzed to elucidate the differences between Sca-1$^-$ and Sca-1$^+$ VM CD8 T cells. Using Enrichr, the top 10 enriched pathways between these two cell types were identified (Figure 17A, Table 9 and 10). A remarkable finding was the enrichment of complement-related pathways, including the *complement cascade*, the *complement activation classical pathway* and the *innate immune system* in Sca-1$^+$ VM CD8 T cells (Figure 17A, upper panel and Table 9). However, enriched pathways upregulated in Sca-1$^-$ (Q1 and Q4) VM subsets did not carry a significant number of DEGs (Table 10). Heatmap analysis revealed higher expression of these complement-related genes in both Sca-1$^+$ VM (Q2 and Q3) and TM cells, whereas their expression was lower in naive and Ly6C$^+$Sca-1$^-$ VM (Q1) cells (Figure 17B). The Ly6C$^-$Sca-1$^-$ VM (Q4) subset exhibited intermediate levels of expression. IFNs are known to induce complement gene expression, and the genes *C1qc*, *C1qb*, and *C1qa*, which are enriched in Sca-1$^+$ VM cells (Figure 17B and Table 9), initiate of the classical complement activation pathway and are upregulated by IFN-α [67]. In addition, it has been reported that IFN-β induces synapse elimination by microglia in mouse models of Alzheimer's disease via a complement-dependent mechanism [68].

Taken together, these findings suggest that complement-related genes serve as a signature for Sca-1^{+} VM (Q2 and Q3) cells, indicating the effects of type I IFN signaling.

A Sca-1^{-} (Q1 and Q4) < Sca-1^{+} (Q2 and Q3), Bioplanet 2019

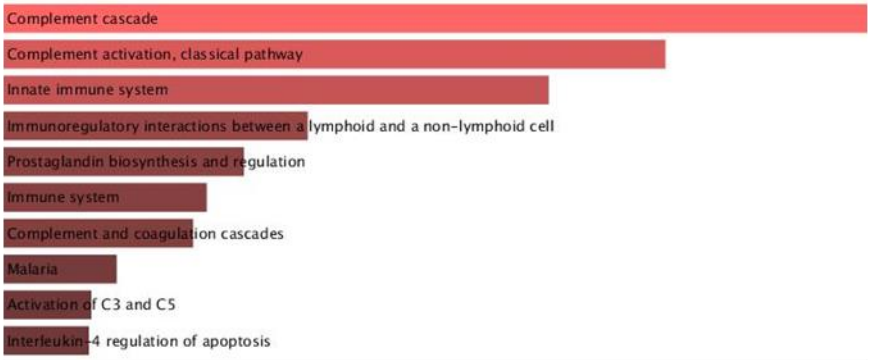

Sca-1^{-} (Q1 and Q4) > Sca-1^{+} (Q2 and Q3), Bioplanet 2019

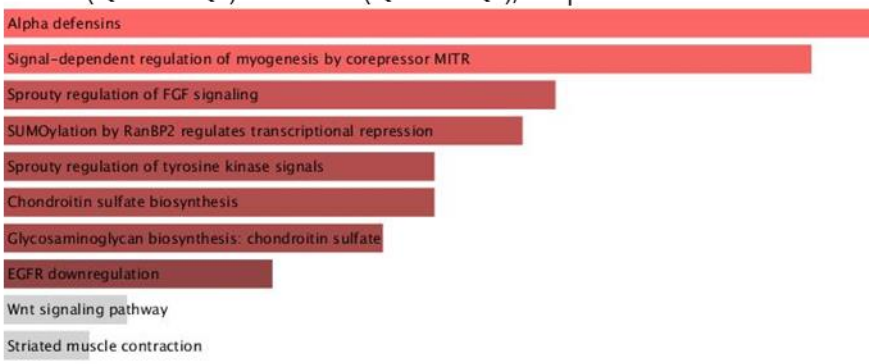

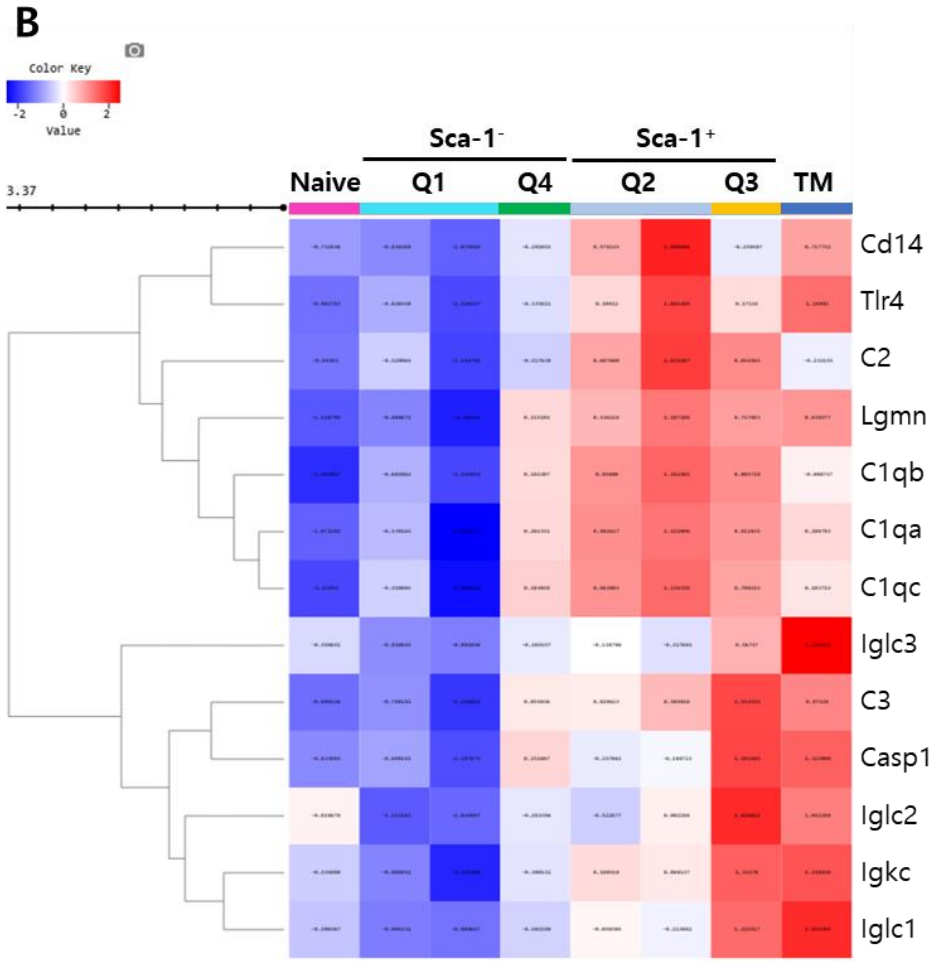

Figure 17. Complement pathway is dominant in Sca-1$^+$ VM CD8 T cells. (A) Using the Bioplanet 2019 tool from the Enrichr website, the top 10 enriched pathways upregulated in Sca-1$^+$ (Q2 and Q3; upper) or Sca-1$^-$ (Q1 and Q4; lower) VM cells. The intensity of color represents the significance of the pathway. (B) The heatmap shows the expression pattern of the genes associated with the top three enriched pathways in Sca-1$^+$ (Q2 and Q3) cells including complement cascade, complement

activation classical pathway, and innate immune system in all subsets of CD8 T cells a heatmap.

Table 9. Upregulated DEGs in Sca-1$^+$ (Q2 and Q3) vs Sca-1$^-$ (Q1 and Q4) CD8 T cell subsets

	Name	P-value	Adjusted P-value	Odds Ratio	Combined Score	Genes
1	Complement cascade	5.16E-09	1.77E-06	18.97538	362.0972	C1QB;C3;C1QA;IGKC;IGLC3;IGLC1;IGLC2;C2;C1QC
2	Complement activation, classical pathway	1.15E-07	1.98E-05	58.2189	930.0143	C1QB;C3;C1QA;C2;C1QC
3	Innate immune system	6.95E-07	7.95E-05	6.197225	87.87048	C1QB;C1QA;C2;C3;IGKC;CASP1;IGLC3;IGLC1;CD14;IGLC2;TLR4;LGMN;C1QC
4	Immunoregulatory interactions between a lymphoid and a non-lymphoid cell	2.83E-05	0.002427	8.812946	92.29443	C3;TYROBP;VCAM1;IGKC;IGLC3;IGLC1;IGLC2
5	Prostaglandin biosynthesis and regulation	7.55E-05	0.005181	20.53976	194.9425	ANXA1;HPGD;TBXAS1;S100A6
6	Immune system	1.34E-04	0.007655	2.861705	25.52158	C1QB;C1QA;VCAM1;SYK;CYBB;C2;C3;TYROBP;IGKC;MRC1;CASP1;IGLC3;CTSH;IGLC1;CD14;IGLC2;TLR4;LGMN;C1QC
7	Complement and coagulation cascades	1.65E-04	0.008091	10.71939	93.35267	C1QB;C3;C1QA;C2;C1QC

8	Malaria	5.35E-04	0.022951	11.78753	88.79168	VCAM1;LRP1;SDC3;TLR4
9	Activation of C3 and C5	7.89E-04	0.02812	68.44483	488.9853	C3;C2
10	Interleukin-4 regulation of apoptosis	8.20E-04	0.02812	4.354101	30.94203	ARHGAP32;VCAM1;FCER1G;ANXA1;GZMA;LPL;GZMB;TLR4

Table 10. Upregulated DEGs in Sca-1$^-$ (Q1 and Q4) vs Sca-1$^+$ (Q2 and Q3) VM CD8 T cell subsets

	Name	P-value	Adjusted P-value	Odds Ratio	Combined Score	Genes
1	Alpha defensins	0.015199	0.196201	75.59848	316.4937	ART1
2	Signal-dependent regulation of myogenesis by corepressor MITR	0.016874	0.196201	67.19529	274.2892	HDAC9
3	Sprouty regulation of FGF signaling	0.026866	0.196201	40.30505	145.7795	SPRY2
4	SUMOylation by RanBP2 regulates transcriptional repression	0.028521	0.196201	37.78409	134.4019	HDAC9
5	Sprouty regulation of tyrosine kinase signals	0.033472	0.196201	31.8134	108.0717	SPRY2
6	Chondroitin sulfate biosynthesis	0.033472	0.196201	31.8134	108.0717	CHST3
7	Glycosaminoglycan biosynthesis: chondroitin sulfate	0.036759	0.196201	28.78066	95.0735	CHST3
8	EGFR downregulation	0.044928	0.196201	23.24009	72.10681	SPRY2
9	Wnt signaling pathway	0.058522	0.196201	5.386736	15.28946	HDAC9;SOX4
10	Striated muscle contraction	0.062665	0.196201	16.32187	45.21077	TMOD1

DISCUSSION

Previous studies have shown that VM CD8 T cells are generated via TCR signaling and cytokine-dependent mechanisms involving IL-4, IL-15, and type I IFN in both the thymus and the periphery [4-6]. However, the specific roles of these cytokines in the development of VM CD8 T cells have yet to be elucidated. In this study, VM CD8 T cells, which were defined as the phenotype of $CD44^{hi}$ and $CD49d^{-}$, were classified into four subsets based on their levels of Ly6C and Sca-1. This classification revealed that the $Ly6C^{+}$ $Sca\text{-}1^{+}$ (Q2) and $Ly6C^{-}$ $Sca\text{-}1^{+}$ (Q3) VM subsets depend primarily on type I IFN for their development, while IL-4 only partially affected the development of the $Ly6C^{+}$ $Sca\text{-}1^{-}$ (Q1) subset. Notably, IL-15 signal-deficient IL-15Rα KO mice exhibited significant reductions in both the $Ly6C^{+}$ $Sca\text{-}1^{-}$ (Q1) and $Ly6C^{+}$ $Sca\text{-}1^{+}$ (Q2) subsets. Analysis of bulk mRNA sequencing data from these VM cell subsets revealed that $Ly6C^{+}$ VM CD8 cells exhibit unique characteristics that distinguish them from $Ly6C^{-}$ VM subsets and true memory cells, including lower expression of cell cycle-related genes and higher expression of IL-15 signal-associated genes. Flow cytometric analysis further supported these findings, and in vitro studies showed that $Ly6C^{+}$ VM CD8 cells are more dependent on IL-15 signaling for their survival compared with the other subsets. $Ly6C^{+}$ VM memory cells also exhibited

greater effector functions compared with Ly6C$^-$ subsets. This suggests that Ly6C$^+$ VM memory cells can mount an immediate response to foreign antigens, similar to innate T cells and true memory T cells. This study also investigated the effect of exogenous IL-4 administration on the protection of mice against lethal influenza infection from the perspective of VM CD8 T cells. Overall, this study provided evidence supporting the heterogeneity of VM CD8 T cells and elucidated the role of cytokines such as type I IFN, IL-4, and IL-15 in the development of each VM subset.

Previously, a two-step hypothesis for VM CD8 T cell generation was proposed [4]. According to this hypothesis, developing CD8 T cells in the first stage are exposed to cytokine signals, including type I IFN, IL-4 and IL-15, leading to the initiation of Runx2, Eomes and IL-2/IL-15Rβ expression. CD8 T cells at this stage are considered to be precursors of VM cells. In the second stage, IL-15, produced by dendritic cells in response to type I IFN, acts on the progenitor VM CD8 T cells, leading to further differentiation and the upregulation of CD44, Eomes and IL-2/IL-15Rβ, ultimately resulting in differentiation into mature VM T cells. In this respect, Ly6C$^+$ VM cells, which showed higher levels of *Runx2*, *Eomes* and *Il2rb* (encoding IL-2/IL-15Rβ) gene expression and superior effector functions compared with Ly6C$^-$ cells, correspond to mature VM cells. In addition, approximately 30% of the Ly6C$^+$ Sca-1$^-$

(Q1) population, which was very rarely detected in IL-15 signal-deficient mice, was still found in IL-4 KO mice. These findings raise the possibility that the population reduced in IL-4 KO mice may originate from IL-4-induced innate CD8 T cells, which also depend on IL-15 for their development. These findings also suggest that IL-15 may play an independent role in the generation of $Ly6C^+$ $Sca\text{-}1^-$ (Q1) VM CD8 T cells even in the absence of IL-4 signaling, such as during the homeostatic proliferative state. However, the reduction in the $Ly6C^+$ $Sca\text{-}1^+$ (Q2) population was more significant in IFNAR1 KO mice than in IL-15α KO mice, with a 25-fold and 3-fold reduction, respectively. This suggests that the $Ly6C^+$ $Sca\text{-}1^+$ (Q2) population consists of both type I IFN- and IL-15 dependent populations and only type I IFN-dependent population. It is also interesting to note that the $Ly6C^+$ $Sca\text{-}1^+$ (Q2) subset showed high expression of IL-4Rα similar to the $Ly6C^+$ $Sca\text{-}1^-$ (Q1) subset, raising the possibility that this population may also be exposed to IL-4 signaling in vivo similar to the $Ly6C^+$ $Sca\text{-}1^-$ (Q1) cells, although not reduced in IL-4 KO mice. Further, this study revealed a significant reduction in the $Ly6C^-$ $Sca\text{-}1^+$ (Q3) subset in mice lacking type I IFN signaling, but not in IL-15Rα KO mice. Type I IFN contributes to the development of VM CD8 cells by inducing IL-15 production in dendritic cells [4]. Therefore, it is plausible that the population reduced in IFNAR1 KO, but not in IL-15Rα KO, could be the type I IFN-induced VM

precursor proposed by the two-step hypothesis. This possibility is further supported by the increase of this population in IL-15Rα KO mice.

The importance of IL-15 signaling in the development of Ly6C$^+$ VM CD8 T cells was further supported by bulk RNA sequencing analysis and in vitro experiments. RNA sequencing analysis revealed that Ly6C$^+$ cells upregulated *il2rb*, *il15ra*, and *runx2* genes while downregulating *bcl6* expression compared with other subsets, including Ly6C$^-$ VM, naïve, and TM cells. Bcl6, known as a regulator of proliferation in follicular helper T cells and B cells, has also been implicated in the maintenance of CD8 T cells [51]. In addition, an in vitro experiment showed that IL-15 trans-presented with cells expressing IL-15Rα, rather than IL-15 alone, induced STAT5 activation and decreased Bcl6 expression [69]. IL-15Rα is expressed on dendritic cells, and the IL-15/IL-15Rα complex has a strong affinity for IL-15Rβ and the common γ chain (IL-2Rγ), facilitating IL-15 signaling [70, 71]. Accordingly, the lower expression of Bcl6 in Ly6C$^+$ VM cells suggests increased sensitivity to IL-15 signaling, possibly due to their higher expression of *Il2rb* and *Il15ra* genes compared with other CD8 T cell subsets. Further, in vitro cell viability assays showed that Ly6C$^+$ VM cells are strongly dependent on IL-15 for their survival compared with other cell populations. Ly6C, known as a memory marker for CD8 T cells, is upregulated by TCR stimulation, and its expression correlates with IFN-γ production [72].

Accordingly, Ly6C^{+} VM CD8 T cells exhibited significantly superior effector functions in terms of IFN-γ and TNF-α production, when compared with Ly6C^{-} VM cells.

Historically, innate T cells that develop from double-positive (CD4^{+}CD8^{+}) thymocytes have been defined as cells expressing activated and/or memory phenotype and exhibit immediate effector functions [1]. In addition, IL-4-dependent innate CD8 T cells exhibit the characteristic CD44^{hi} CXCR3^{+} phenotype [8]. However, VM T cells were initially defined solely on the basis of their CD44^{hi} CD49d^{-} memory-like phenotype [4], and the expression of CXCR3 molecules was observed in both IL-4- and type I IFN-dependent VM CD8 T cells [7, 19]. The current study demonstrated the phenotypic and functional heterogeneity of CD44^{hi} CD49d^{-} VM CD8 T cells. Notably, only Ly6C^{+} VM CD8 T cells showed immediate effector function upon TCR stimulation. Interestingly, CXCR3 expression was predominantly found on Ly6C^{+} VM cells and low in other subsets of CD8 T cells. These findings suggest that only the Ly6C^{+} or CXCR3^{+} population of VM CD8 T cells can be considered functionally equivalent to innate CD8 T cells.

This study demonstrated the usefulness of Sca-1 as a marker for distinguishing the type I IFN-dependent VM subset from its IL-4-dependent counterpart. Similar to Ly6C, Sca-1 is expressed on memory T cells rather than naïve T cells, and its expression increases significantly

during viral infection [25]. Nonetheless, Sca-1 does not appear to be essential for the development and function of memory T cells, as reported previously indicating that the number and quality of memory T cells were unaffected in Sca-1 KO mouse models [25]. To investigate the impact of type I IFN signaling on VM CD8 T cells, this study identified DEGs between Sca-1^+ and Sca-1^- VM CD8 T cells, and the complement cascade pathway was expressed significantly.

In this study, pre-treatment of IL-4 in a complex form with anti-IL-4 antibody (IL-4C) was found to protect mice from influenza-associated mortality. This treatment also promoted the migration of both antigen-specific and bystander CD8 T cells into the infected lungs, depending on the increased expression of CXCR3 in CD8 T cells. However, no significant differences in viral titers were observed between IL-4-pretreated and control mice. Further, IL-4 treatment unexpectedly increased CXCR3 expression only in naive and Ly6C^- VM CD8 T cells and expanded only Ly6C^- VM CD8 T cells, but did not affect Ly6C^+ cells that exhibit a superior effector function. This suggests that survival observed in IL-4-treated mice following influenza infection may not be attributed to increased effector function of CD8 T cells. Severe influenza infection is associated with lung epithelial damage due to excessive infiltration of inflammatory cells, particularly neutrophils and monocytes [73]. Previous studies have reported that IL-4 administration

alleviates lung damage via macrophage reprogramming in models of acute lung injury [74]. In addition, IL-4 promoted lung epithelial cell regeneration in sepsis-induced acute lung injury by polarizing macrophages to the M2 type. IL-4 has also been shown to attenuate neutrophil migration into inflamed tissue [75, 76]. IL-4Rα signaling suppresses acute lung injury by inhibiting neutrophil survival [77]. Given these findings, it is plausible that exogenous IL-4 treatment may prevent lung injury by inducing macrophage M2 polarization and/or limiting neutrophil infiltration or survival, although significant differences in the number of macrophages and neutrophils in infected lungs were found between IL-4C-treated and control mice. Further, it would be interesting to investigate the regulatory role of Ly6C$^-$ VM CD8 T cells in this context.

This study has certain limitations, as it did not fully elucidate how cytokines such as type I IFN, IL-4, and IL-15 work together to induce the development and/or expansion of VM cells. Additionally, it did not explore the possibility that IL-4 administration may protect against lethal influenza infection by affecting non-T cell components. Nevertheless, this study represents the first of its kind to elucidate the heterogeneity of VM CD8 T cells and the involvement of cytokines, including type I IFN, IL-4, and IL-15, in the development of distinct VM subsets.

REFERENCES

[1] L.J. Berg, Signalling through TEC kinases regulates conventional versus innate CD8(+) T-cell development, Nat Rev Immunol 7(6) (2007) 479-85.

[2] A. Veillette, Z. Dong, S. Latour, Consequence of the SLAM-SAP signaling pathway in innate-like and conventional lymphocytes, Immunity 27(5) (2007) 698-710.

[3] Y.J. Lee, S.C. Jameson, K.A. Hogquist, Alternative memory in the CD8 T cell lineage, Trends Immunol 32(2) (2011) 50-6.

[4] T. Hussain, K.M. Quinn, Similar but different: virtual memory CD8 T cells as a memory-like cell population, Immunol Cell Biol 97(7) (2019) 675-684.

[5] G. Lauvau, S. Goriely, Memory CD8+ T Cells: Orchestrators and Key Players of Innate Immunity?, PLoS Pathog 12(9) (2016) e1005722.

[6] M. Pribikova, A. Moudra, O. Stepanek, Opinion: Virtual memory CD8 T cells and lymphopenia-induced memory CD8 T cells represent a single subset: Homeostatic memory T cells, Immunol Lett 203 (2018) 57-61.

[7] V. Martinet, S. Tonon, D. Torres, A. Azouz, M. Nguyen, A. Kohler, V. Flamand, C.A. Mao, W.H. Klein, O. Leo, S. Goriely, Type I interferons regulate eomesodermin expression and the development of unconventional memory CD8(+) T cells, Nat Commun 6 (2015) 7089.

[8] M.A. Weinreich, O.A. Odumade, S.C. Jameson, K.A. Hogquist, T cells expressing the transcription factor PLZF regulate the development of memory-like CD8+ T cells, Nat Immunol 11(8) (2010) 709-16.

[9] L.O. Atherly, J.A. Lucas, M. Felices, C.C. Yin, S.L. Reiner, L.J. Berg, The Tec family tyrosine kinases Itk and Rlk regulate the development of conventional CD8+ T cells, Immunity 25(1) (2006) 79-91.

[10] C. Broussard, C. Fleischacker, R. Horai, M. Chetana, A.M. Venegas, L.L. Sharp, S.M. Hedrick, B.J. Fowlkes, P.L. Schwartzberg, Altered development of CD8+ T cell lineages in mice deficient for the Tec kinases Itk and Rlk, Immunity 25(1) (2006) 93-104.

[11] A.D. Akue, J.Y. Lee, S.C. Jameson, Derivation and maintenance of virtual memory CD8 T cells, J Immunol 188(6) (2012) 2516-23.

[12] C. Haluszczak, A.D. Akue, S.E. Hamilton, L.D. Johnson, L. Pujanauski, L. Teodorovic, S.C. Jameson, R.M. Kedl, The antigen-specific CD8+ T cell repertoire in unimmunized mice includes memory phenotype cells bearing markers of homeostatic expansion, J Exp Med 206(2) (2009) 435-48.

[13] J.T. White, E.W. Cross, M.A. Burchill, T. Danhorn, M.D. McCarter, H.R. Rosen, B. O'Connor, R.M. Kedl, Virtual memory T cells develop and mediate bystander protective immunity in an IL-15-dependent manner, Nat Commun 7 (2016) 11291.

[14] J.Y. Lee, S.E. Hamilton, A.D. Akue, K.A. Hogquist, S.C. Jameson,

Virtual memory CD8 T cells display unique functional properties, Proc Natl Acad Sci U S A 110(33) (2013) 13498-503.

[15] L. Van Kaer, Innate and virtual memory T cells in man, Eur J Immunol 45(7) (2015) 1916-20.

[16] F. Jacomet, E. Cayssials, S. Basbous, A. Levescot, N. Piccirilli, D. Desmier, A. Robin, A. Barra, C. Giraud, F. Guilhot, L. Roy, A. Herbelin, J.M. Gombert, Evidence for eomesodermin-expressing innate-like CD8(+) KIR/NKG2A(+) T cells in human adults and cord blood samples, Eur J Immunol 45(7) (2015) 1926-33.

[17] J.T. White, E.W. Cross, R.M. Kedl, Antigen-inexperienced memory CD8(+) T cells: where they come from and why we need them, Nat Rev Immunol 17(6) (2017) 391-400.

[18] J.R. Groom, A.D. Luster, CXCR3 in T cell function, Exp Cell Res 317(5) (2011) 620-31.

[19] K.R. Renkema, J.Y. Lee, Y.J. Lee, S.E. Hamilton, K.A. Hogquist, S.C. Jameson, IL-4 sensitivity shapes the peripheral CD8+ T cell pool and response to infection, J Exp Med 213(7) (2016) 1319-29.

[20] E. Ventre, L. Brinza, S. Schicklin, J. Mafille, C.A. Coupet, A. Marcais, S. Djebali, V. Jubin, T. Walzer, J. Marvel, Negative regulation of NKG2D expression by IL-4 in memory CD8 T cells, J Immunol 189(7) (2012) 3480-9.

[21] H.J. Park, A. Lee, J.I. Lee, S.H. Park, S.J. Ha, K.C. Jung, Effect of

IL-4 on the Development and Function of Memory-like CD8 T Cells in the Peripheral Lymphoid Tissues, Immune Netw 16(2) (2016) 126-33.

[22] S.C. Jameson, Y.J. Lee, K.A. Hogquist, Innate memory T cells, Adv Immunol 126 (2015) 173-213.

[23] J.H. DeLong, A.O. Hall, C. Konradt, G.M. Coppock, J. Park, G. Harms Pritchard, C.A. Hunter, Cytokine- and TCR-Mediated Regulation of T Cell Expression of Ly6C and Sca-1, J Immunol 200(5) (2018) 1761-1770.

[24] Y.J. Ju, S.W. Lee, Y.C. Kye, G.W. Lee, H.O. Kim, C.H. Yun, J.H. Cho, Self-reactivity controls functional diversity of naive CD8(+) T cells by co-opting tonic type I interferon, Nat Commun 12(1) (2021) 6059.

[25] J.K. Whitmire, B. Eam, J.L. Whitton, Mice deficient in stem cell antigen-1 (Sca1, Ly-6A/E) develop normal primary and memory CD4+ and CD8+ T-cell responses to virus infection, Eur J Immunol 39(6) (2009) 1494-504.

[26] W.W. Thompson, L. Comanor, D.K. Shay, Epidemiology of seasonal influenza: use of surveillance data and statistical models to estimate the burden of disease, J Infect Dis 194 Suppl 2 (2006) S82-91.

[27] R.R. Thangavel, N.M. Bouvier, Animal models for influenza virus pathogenesis, transmission, and immunology, J Immunol Methods 410 (2014) 60-79.

[28] A. Lee, S.P. Park, C.H. Park, B.H. Kang, S.H. Park, S.J. Ha, K.C.

Jung, IL-4 Induced Innate CD8+ T Cells Control Persistent Viral Infection, PLoS Pathog 11(10) (2015) e1005193.

[29] K.C. Pang, M.T. Sanders, J.J. Monaco, P.C. Doherty, S.J. Turner, W. Chen, Immunoproteasome subunit deficiencies impact differentially on two immunodominant influenza virus-specific CD8+ T cell responses, J Immunol 177(11) (2006) 7680-8.

[30] S.C. Morris, S.M. Heidorn, D.R. Herbert, C. Perkins, D.A. Hildeman, M.V. Khodoun, F.D. Finkelman, Endogenously produced IL-4 nonredundantly stimulates CD8+ T cell proliferation, J Immunol 182(3) (2009) 1429-38.

[31] A. Baer, K. Kehn-Hall, Viral concentration determination through plaque assays: using traditional and novel overlay systems, J Vis Exp (93) (2014) e52065.

[32] H.M. Ibrahim, M. Nishimura, S. Tanaka, W. Awadin, H. Furuoka, X. Xuan, Y. Nishikawa, Overproduction of Toxoplasma gondii cyclophilin-18 regulates host cell migration and enhances parasite dissemination in a CCR5-independent manner, BMC Microbiol 14 (2014) 76.

[33] A. Giulietti, L. Overbergh, D. Valckx, B. Decallonne, R. Bouillon, C. Mathieu, An overview of real-time quantitative PCR: applications to quantify cytokine gene expression, Methods 25(4) (2001) 386-401.

[34] G. Grodeland, M. Baranowska-Hustad, J. Abadejos, T.R. Blane, J. Teijaro, D. Nemazee, B. Bogen, Induction of Cross-Reactive and

Protective Antibody Responses After DNA Vaccination With MHCII-Targeted Stem Domain From Influenza Hemagglutinin, Front Immunol 11 (2020) 431.

[35] A.M. Bolger, M. Lohse, B. Usadel, Trimmomatic: a flexible trimmer for Illumina sequence data, Bioinformatics 30(15) (2014) 2114-20.

[36] D. Kim, B. Langmead, S.L. Salzberg, HISAT: a fast spliced aligner with low memory requirements, Nat Methods 12(4) (2015) 357-60.

[37] M. Pertea, G.M. Pertea, C.M. Antonescu, T.C. Chang, J.T. Mendell, S.L. Salzberg, StringTie enables improved reconstruction of a transcriptome from RNA-seq reads, Nat Biotechnol 33(3) (2015) 290-5.

[38] M. Pertea, D. Kim, G.M. Pertea, J.T. Leek, S.L. Salzberg, Transcript-level expression analysis of RNA-seq experiments with HISAT, StringTie and Ballgown, Nat Protoc 11(9) (2016) 1650-67.

[39] M.D. Robinson, D.J. McCarthy, G.K. Smyth, edgeR: a Bioconductor package for differential expression analysis of digital gene expression data, Bioinformatics 26(1) (2010) 139-40.

[40] E.Y. Chen, C.M. Tan, Y. Kou, Q. Duan, Z. Wang, G.V. Meirelles, N.R. Clark, A. Ma'ayan, Enrichr: interactive and collaborative HTML5 gene list enrichment analysis tool, BMC Bioinformatics 14 (2013) 128.

[41] M.V. Kuleshov, M.R. Jones, A.D. Rouillard, N.F. Fernandez, Q. Duan, Z. Wang, S. Koplev, S.L. Jenkins, K.M. Jagodnik, A. Lachmann, M.G. McDermott, C.D. Monteiro, G.W. Gundersen, A. Ma'ayan, Enrichr:

a comprehensive gene set enrichment analysis web server 2016 update, Nucleic Acids Res 44(W1) (2016) W90-7.

[42] Z. Xie, A. Bailey, M.V. Kuleshov, D.J.B. Clarke, J.E. Evangelista, S.L. Jenkins, A. Lachmann, M.L. Wojciechowicz, E. Kropiwnicki, K.M. Jagodnik, M. Jeon, A. Ma'ayan, Gene Set Knowledge Discovery with Enrichr, Curr Protoc 1(3) (2021) e90.

[43] F.D. Finkelman, K.B. Madden, S.C. Morris, J.M. Holmes, N. Boiani, I.M. Katona, C.R. Maliszewski, Anti-cytokine antibodies as carrier proteins. Prolongation of in vivo effects of exogenous cytokines by injection of cytokine-anti-cytokine antibody complexes, J Immunol 151(3) (1993) 1235-44.

[44] T.S. Kim, E.C. Shin, The activation of bystander CD8(+) T cells and their roles in viral infection, Exp Mol Med 51(12) (2019) 1-9.

[45] A.D. Judge, X. Zhang, H. Fujii, C.D. Surh, J. Sprent, Interleukin 15 controls both proliferation and survival of a subset of memory-phenotype CD8(+) T cells, J Exp Med 196(7) (2002) 935-46.

[46] S.Y. Lee, C. Jang, K.A. Lee, Polo-like kinases (plks), a key regulator of cell cycle and new potential target for cancer therapy, Dev Reprod 18(1) (2014) 65-71.

[47] V. Krenn, A. Musacchio, The Aurora B Kinase in Chromosome Bi-Orientation and Spindle Checkpoint Signaling, Front Oncol 5 (2015) 225.

[48] D.G. Johnson, R. Schneider-Broussard, Role of E2F in cell cycle

control and cancer, Front Biosci 3 (1998) d447-8.

[49] I.H. Seo, H.S. Eun, J.K. Kim, H. Lee, S. Jeong, S.J. Choi, J. Lee, B.S. Lee, S.H. Kim, W.S. Rou, D.H. Lee, W. Kim, S.H. Park, E.C. Shin, IL-15 enhances CCR5-mediated migration of memory CD8(+) T cells by upregulating CCR5 expression in the absence of TCR stimulation, Cell Rep 36(4) (2021) 109438.

[50] J.C. Nolz, Molecular mechanisms of CD8(+) T cell trafficking and localization, Cell Mol Life Sci 72(13) (2015) 2461-73.

[51] H. Ichii, A. Sakamoto, M. Hatano, S. Okada, H. Toyama, S. Taki, M. Arima, Y. Kuroda, T. Tokuhisa, Role for Bcl-6 in the generation and maintenance of memory CD8+ T cells, Nat Immunol 3(6) (2002) 558-63.

[52] B.A. Khalil, N.M. Elemam, A.A. Maghazachi, Chemokines and chemokine receptors during COVID-19 infection, Comput Struct Biotechnol J 19 (2021) 976-988.

[53] X. Wang, X.Y. Zhao, Transcription Factors Associated With IL-15 Cytokine Signaling During NK Cell Development, Front Immunol 12 (2021) 610789.

[54] S. Ma, M.A. Caligiuri, J. Yu, Harnessing IL-15 signaling to potentiate NK cell-mediated cancer immunotherapy, Trends Immunol 43(10) (2022) 833-847.

[55] T.A. Waldmann, M.D. Miljkovic, K.C. Conlon, Interleukin-15

(dys)regulation of lymphoid homeostasis: Implications for therapy of autoimmunity and cancer, J Exp Med 217(1) (2020).

[56] E. Olesin, R. Nayar, P. Saikumar-Lakshmi, L.J. Berg, The Transcription Factor Runx2 Is Required for Long-Term Persistence of Antiviral CD8(+) Memory T Cells, Immunohorizons 2(7) (2018) 251-261.

[57] W. Zhao, H. Yang, J. Chai, L. Xing, RUNX2 as a promising therapeutic target for malignant tumors, Cancer Manag Res 13 (2021) 2539-2548.

[58] A.M. Intlekofer, N. Takemoto, E.J. Wherry, S.A. Longworth, J.T. Northrup, V.R. Palanivel, A.C. Mullen, C.R. Gasink, S.M. Kaech, J.D. Miller, L. Gapin, K. Ryan, A.P. Russ, T. Lindsten, J.S. Orange, A.W. Goldrath, R. Ahmed, S.L. Reiner, Effector and memory CD8+ T cell fate coupled by T-bet and eomesodermin, Nat Immunol 6(12) (2005) 1236-44.

[59] E.L. Pearce, A.C. Mullen, G.A. Martins, C.M. Krawczyk, A.S. Hutchins, V.P. Zediak, M. Banica, C.B. DiCioccio, D.A. Gross, C.A. Mao, H. Shen, N. Cereb, S.Y. Yang, T. Lindsten, J. Rossant, C.A. Hunter, S.L. Reiner, Control of effector CD8+ T cell function by the transcription factor Eomesodermin, Science 302(5647) (2003) 1041-3.

[60] A. Allam, D.B. Conze, M.L. Giardino Torchia, I. Munitic, H. Yagita, R.T. Sowell, A.L. Marzo, J.D. Ashwell, The CD8+ memory T-cell state

of readiness is actively maintained and reversible, Blood 114(10) (2009) 2121-30.

[61] L. Van Kaer, S. Joyce, Survivre et vivre: When iNKT cells met a Hippo, J Exp Med 217(6) (2020).

[62] J.L. Raynor, C. Liu, Y. Dhungana, C. Guy, N.M. Chapman, H. Shi, G. Neale, H. Sesaki, H. Chi, Hippo/Mst signaling coordinates cellular quiescence with terminal maturation in iNKT cell development and fate decisions, J Exp Med 217(6) (2020).

[63] D.A. Witherden, R. Boismenu, W.L. Havran, CD81 and CD28 costimulate T cells through distinct pathways, J Immunol 165(4) (2000) 1902-9.

[64] J. Son, S.J. Ha, Extrinsic Acquisition of CD80 by Antigen-Specific CD8(+) T Cells Regulates Their Recall Immune Responses to Acute Viral Infection, Immune Netw 19(4) (2019) e25.

[65] C.E. Zuber, J.P. Galizzi, A. Valle, N. Harada, M. Howard, J. Banchereau, Interleukin 4 receptors on normal human B lymphocytes: characterization and regulation, Eur J Immunol 20(3) (1990) 551-5.

[66] H. Renz, J. Domenico, E.W. Gelfand, IL-4-dependent up-regulation of IL-4 receptor expression in murine T and B cells, J Immunol 146(9) (1991) 3049-55.

[67] S. Jodele, M. Medvedovic, N. Luebbering, J. Chen, C.E. Dandoy, B.L. Laskin, S.M. Davies, Interferon-complement loop in transplant-

associated thrombotic microangiopathy, Blood Adv 4(6) (2020) 1166-1177.

[68] E.R. Roy, B. Wang, Y.W. Wan, G. Chiu, A. Cole, Z. Yin, N.E. Propson, Y. Xu, J.L. Jankowsky, Z. Liu, V.M. Lee, J.Q. Trojanowski, S.D. Ginsberg, O. Butovsky, H. Zheng, W. Cao, Type I interferon response drives neuroinflammation and synapse loss in Alzheimer disease, J Clin Invest 130(4) (2020) 1912-1930.

[69] I.D. Cooley, K.A. Read, K.J. Oestreich, Trans-presentation of IL-15 modulates STAT5 activation and Bcl-6 expression in TH1 cells, Sci Rep 5 (2015) 15722.

[70] E.F. Castillo, K.S. Schluns, Regulating the immune system via IL-15 transpresentation, Cytokine 59(3) (2012) 479-90.

[71] S. Dubois, J. Mariner, T.A. Waldmann, Y. Tagaya, IL-15Ralpha recycles and presents IL-15 In trans to neighboring cells, Immunity 17(5) (2002) 537-47.

[72] T.L. Walunas, D.S. Bruce, L. Dustin, D.Y. Loh, J.A. Bluestone, Ly-6C is a marker of memory CD8+ T cells, J Immunol 155(4) (1995) 1873-83.

[73] L.A. Perrone, J.K. Plowden, A. Garcia-Sastre, J.M. Katz, T.M. Tumpey, H5N1 and 1918 pandemic influenza virus infection results in early and excessive infiltration of macrophages and neutrophils in the lungs of mice, PLoS Pathog 4(8) (2008) e1000115.

[74] F.R. D'Alessio, J.M. Craig, B.D. Singer, D.C. Files, J.R. Mock, B.T. Garibaldi, J. Fallica, A. Tripathi, P. Mandke, J.H. Gans, N. Limjunyawong, V.K. Sidhaye, N.M. Heller, W. Mitzner, L.S. King, N.R. Aggarwal, Enhanced resolution of experimental ARDS through IL-4-mediated lung macrophage reprogramming, Am J Physiol Lung Cell Mol Physiol 310(8) (2016) L733-46.

[75] J. Woytschak, N. Keller, C. Krieg, D. Impellizzieri, R.W. Thompson, T.A. Wynn, A.S. Zinkernagel, O. Boyman, Type 2 Interleukin-4 Receptor Signaling in Neutrophils Antagonizes Their Expansion and Migration during Infection and Inflammation, Immunity 45(1) (2016) 172-84.

[76] F. Chen, Z. Liu, W. Wu, C. Rozo, S. Bowdridge, A. Millman, N. Van Rooijen, J.F. Urban, Jr., T.A. Wynn, W.C. Gause, An essential role for TH2-type responses in limiting acute tissue damage during experimental helminth infection, Nat Med 18(2) (2012) 260-6.

[77] A.J. Harris, A.S. Mirchandani, R.W. Lynch, F. Murphy, L. Delaney, D. Small, P. Coelho, E.R. Watts, P. Sadiku, D. Griffith, R.S. Dickinson, E. Clark, J.A. Willson, T. Morrison, M. Mazzone, P. Carmeliet, B. Ghesquiere, C. O'Kane, D. McAuley, S.J. Jenkins, M.K.B. Whyte, S.R. Walmsley, IL4Ralpha Signaling Abrogates Hypoxic Neutrophil Survival and Limits Acute Lung Injury Responses In Vivo, Am J Respir Crit Care Med 200(2) (2019) 235-246.

국문 초록

일반적인 기억 T 세포는 항원에 노출시 유도되며 기억세포의 표현형을 갖는다. 그러나 흉선 및 말초기관에서 기억세포의 특징을 갖으면서 사이토카인 분비가 빠르게 나타나는 선천 T 세포, 혹은 가상기억 세포라 불리는 CD8 T 세포가 존재함이 확인되었다. 본 논문에서는 여러 사이토카인에 의해 유도되는 가상기억 CD8 T 세포의 기능과 그 발달을 확인하고자 한다. 인터류킨-4 복합체 주입시, 마우스 생체내 가상기억 CD8 T 세포가 유도되며 CXCR3 을 높게 발현하여 바이러스에 특이적인 CD8 T 세포, 방관자 (Bystander) CD8 T 세포 및 미감작세포의 이동을 용이하게 하였다. 가상기억세포의 발달에 미치는 제 1 형 인터페론, 인터류킨-4, 인터류킨-15 의 역할을 확인하기 위하여 가상기억세포를 Ly6C 와 Sca-1 으로 나누어 각각의 유전자결핍 마우스모델에서 확인하였다. 제 1 형 인터류킨 결핍 마우스에서는 Sca-1 을 발현하는 가상기억 CD8 T 세포가 크게 감소하며 인터류킨-15 결핍모델에서는 Ly6C 를 발현하는 가상기억 CD8 T 세포가 줄어들었다. RNA-염기서열분석을 통해 Ly6C 를 발현하는 가상기억 CD8 T

세포는 인터류킨-15 와 관련된 유전자 (인터류킨-2 수용체 베타, 인터류킨-15 수용체 알파)나 기억세포 관련 유전자 (RUNX2, EOMES) 등을 높게 내는 반면 Ly6C 를 발현하지 않는 가상기억 CD8 T 세포는 세포분열과 관련된 유전자를 높게 발현함을 확인하였고, *Mst1* 역시 Ly6C 발현하는 가상기억 CD8 T 세포에서 높게 발현하였다.

주요어 : 인터류킨-4, 제 1 형 인터페론, 인터류킨-15, 가상기억 CD8 T 세포, 인플루엔자 바이러스 A, CXCR3

학 번 : 2016-30010